

UNCLASSIFIED

AD NUMBER
AD913687
NEW LIMITATION CHANGE
TO Approved for public release, distribution unlimited
FROM Distribution authorized to U.S. Gov't. agencies only; Test and Evaluation; JUN 1973. Other requests shall be referred to Air Force Avionics Lab., AFSC, Wright-Patterson AFB, OH.
AUTHORITY
WL/IST ltr, 23 May 1991

THIS PAGE IS UNCLASSIFIED

THIS REPORT HAS BEEN DELIMITED
AND CLEARED FOR PUBLIC RELEASE
UNDER DOD DIRECTIVE 5200.20 AND
NO RESTRICTIONS ARE IMPOSED UPON
ITS USE AND DISCLOSURE.

DISTRIBUTION STATEMENT A

APPROVED FOR PUBLIC RELEASE;
DISTRIBUTION UNLIMITED.

AFAL-TR-73-242

AD 913687

INTEGRATED NAVIGATION SATELLITE/INERTIAL SYSTEM FLIGHT TEST ANALYSIS

Joseph A. D'Appolito

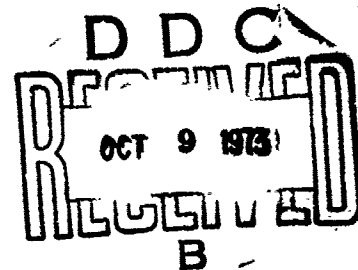
Kenneth J. Roy

THE ANALYTIC SCIENCES CORPORATION

Technical Report AFAL-TR-73-242

5 April 1973

Distribution is limited to U.S. Government Agencies only. Reason: Test and Evaluation. Date Statement Applied: June 1973. Other requests for this document must be referred to: AFAL (NVA/666A), WPAFB, OHIO 45433.



AIR FORCE AVIONICS LABORATORY
Air Force Systems Command
Wright-Patterson Air Force Base
Ohio 45433

NOTICE

When Government drawings, specifications, or other data are used for any purpose other than in connection with a definitely related Government procurement operation, the United States Government thereby incurs no responsibility nor any obligation whatsoever; and the fact that the government may have formulated, furnished, or in any way supplied the said drawings, specifications, or other data, is not to be regarded by implication or otherwise as in any manner licensing the holder or any other person or corporation, or conveying any rights or permission to manufacture, use, or sell any patented invention that may in any way be related thereto.

Copies of this report should not be returned unless return is required by security considerations, contractual obligations, or notice on a specific document.

INTEGRATED NAVIGATION SATELLITE/INERTIAL SYSTEM FLIGHT TEST ANALYSIS

Joseph A. D'Appolito

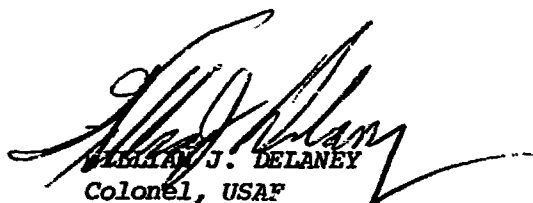
Kenneth J. Roy

Distribution is limited to U.S. Government Agencies only. Reason: Test and Evaluation. Date Statement Applied: June 1973. Other requests for this document must be referred to: AFAL (NVA/866A), WPAFB, OHIO 45433.

FOREWORD

The Analytic Sciences Corporation (TASC), 6 Jacob Way, Reading, Mass. 01867 is presently conducting Integrated Navigation-Satellite Inertial system analysis studies in support of Air Force Avionics Laboratory development efforts. The work reported in this document was conducted from March 1972 through January 1973 as part of Task 02 of Advanced Development Program 666A under Air Force Contract F33615-72-C-1918. The preliminary draft of this report was prepared as TASC Report No. TR 332-1 and submitted for review on 24 May 1973. The authors acknowledge the assistance of the Air Force Project Engineers Capt. Maurice Carr and Capt. Stephen Schwam (NVA/666A).

This technical report has been reviewed and is approved for publication.


WILLIAM J. DELANEY
Colonel, USAF
Chief, Navigation &
Weapon Delivery Division

ABSTRACT

A simulation of an integrated airborne 621B Satellite/Inertial navigation system is planned in which a ground-based beacon configuration will be used in place of the satellites. The TRW Systems Group has designed and built an Integrated Navigation Satellite/Inertial (INI) system and will participate in a test of this equipment for the Air Force Avionics Laboratory at the White Sands Missile Range test center.

This study represents a continuation of an earlier INI flight test support study conducted by TASC. In this study the INI reference system error model is first revised to include the most current data on inertial system and beacon errors. Then an 18-state INI Kalman filter for integrating beacon receiver and inertial data is described. The filter is evaluated in a performance study which includes a comparison against an optimally integrated INI system using a complete 33-state reference error model. Special attention is focused on the conventional baroaltimeter damped vertical channel mechanization proposed by TRW and the problem of filter initialization. A component error budget is generated for the 18-state Kalman filter to identify major sources of system error and filter sensitivity to those errors. A brief review of the TRW flight test program is then presented. An 18-state INI Kalman filter is recommended for initial use in the flight tests and certain additions to the real time flight test data display and diagnostics are suggested.

TABLE OF CONTENTS

	<u>Page No.</u>
1. INTRODUCTION	1-1
1.1 Background and Purpose	1-1
1.2 Report Overview	1-3
2. A REVISED INI REFERENCE ERROR MODEL AND KALMAN FILTER DESIGN	2-1
2.1 An Updated INI Reference Error Model	2-1
2.2 The Vertical Channel Mechanization	2-7
2.3 An 18-State INI Kalman Filter	2-11
3. 18-STATE BEACON/INERTIAL KALMAN FILTER PERFORMANCE EVALUATION	3-1
3.1 Baseline Optimal and 18-State Filter Comparison	3-1
3.2 The Component Error Budget for the 18-State Filter	3-3
3.3 Comparison of Previous Results and Current Studies	3-15
3.4.1 Initialization Study No. 1	3-17
3.4.2 Initialization Study No. 2	3-21
3.5 Performance Evaluation Summary	3-24
4. TRW INI TEST PLAN REVIEW	4-1
5. SUMMARY AND RECOMMENDATIONS	5-1
APPENDIX A - STATE SPACE SPECIFICATION OF THE INI REFERENCE ERROR MODEL	A-1
A.1 Introduction	A-1
A.2 Reference System F and Q Matrices	A-2
A.3 Reference System H and R Matrices	A-7

TABLE OF CONTENTS (Continued)

	<u>Page No.</u>
APPENDIX B - SPECIFICATION OF THE 18-STATE INI KALMAN FILTER DESIGN MODEL	B-1
B.1 Introduction	B-1
B.2 The 18-State INI Kalman Filter Design Model	B-2
REFERENCES	R-1

LIST OF FIGURES

<u>Figure No.</u>		<u>Page No.</u>
1.1-1	The INI Test Configuration	1-1
2.1-1	Accelerometer Misalignments in the Plane of the Level Accelerometer Axes	2-6
2.2-1	INI Vertical Channel Mechanization	2-8
2.2-2	Vertical Channel Error Block Diagram	2-11
2.3-1	INI Kalman Filter Mechanization (Conventional Vertical Channel)	2-14
3.1-1	Beacon/Inertial Test Flight Profile	3-2
3.1-2	Comparison of rms Heading, North Position and North Velocity Errors of the Optimal, and 18-State Filters	3-3
3.1-3	Comparison of rms Altimeter Bias and User Relative Clock Errors in the Optimal and 18-State Filters	3-4
3.2-1	Position Error Budget Histograms for the 18-State INI Filter ($T = 720$ sec)	3-10
3.2-2	Velocity Error Budget Histograms for the 18-State INI Filter ($T = 720$ sec)	3-10
3.2-3	Heading and User-Clock Error Budget Histograms for the 18-State INI Kalman Filter ($T = 720$ sec)	3-10
3.2-4	System Errors Produced by Accelerometer Scale Factor Errors	3-14
3.4-1	Scenario for Initialization Study No. 1	3-18
3.4-2	Scenario for Initialization Study No. 2	3-22

LIST OF TABLES

<u>Table No.</u>		<u>Page No.</u>
2.1-1	INI System Reference Error Model Comparisons	2-2
2.1-2	Beacon/Inertial System Reference Error Model State Complement	2-4
2.3-1	State Vector for the 18-State INI Filter Design Model	2-13
3.1-1	Optimal and 18-State Filter Performance Comparison During Beacon Measurement Phase	3-6
3.1-2	Comparison of Steady State Damped Vertical Channel Response in Aided and Unaided Modes (18-State Kalman Filter)	3-7
3.2-1	Component Error Budget for the 18-State INI Kalman Filter	3-9
3.3-1	Comparison of Current and Previous Results for INI System Performance Predictions (at T = 1080 Secs)	3-16
3.4-1	Initialization Study No. 1 rms Initial Values for 18-State Filter	3-19
3.4-2	Initialization Study No. 1 - Optimal and 18-State Filter Performance Comparison	3-20
3.4-3	Filter Initialization Study No. 2 - Optimal and 18-State Filter Performance Comparison	3-23
B.2-1	Diagonal Elements of the Q^* Matrix for the 18-State Filter	B-4
B.2-2	Design Values for 18-State Filter White Measurement Noises	B-5

1.

INTRODUCTION

1.1 BACKGROUND AND PURPOSE

A simulation of an integrated airborne 621B Satellite/Inertial navigation system is planned in which a ground-based beacon configuration will be used in place of the satellites. The test configuration concept is illustrated in Fig. 1.1-1. The TRW Systems Group has designed and built an Integrated Navigation Satellite/Inertial (INI) system and will participate in a test of this equipment for the Air Force Avionics Laboratory (AFAL) at the White Sands Missile Range (WSMR) test center.

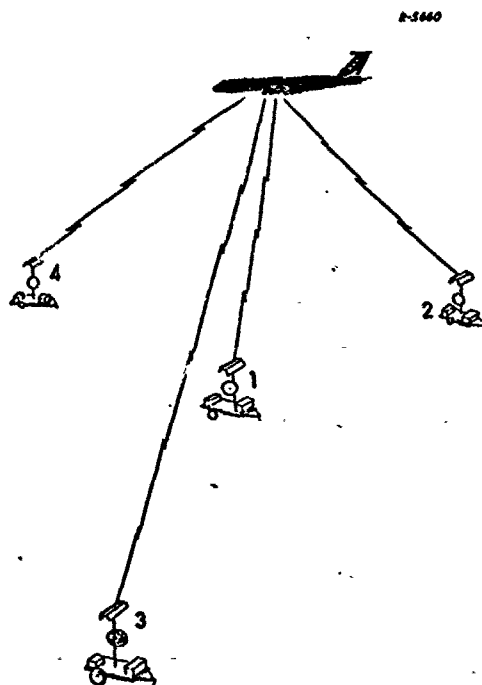


Figure 1.1-1 The INI Test Configuration

In these tests a Kalman filter algorithm will be used to integrate data from the inertial system and a single channel time multiplexed beacon receiver. Under contract to AFAL, The Analytic Sciences Corporation (TASC) recently completed a preliminary INI Kalman filter design study. This study included the formulation of a complete reference error model for the INI system and the design and evaluation of two reduced-state INI Kalman filters. The results of this study are reported in Ref. 1.

The work reported herein is a continuation of the TASC study cited above. The goals of the present study are to:

- Establish the latest best estimates of all INI error sources and refine the INI reference system error model accordingly.
- Optimize an INI Kalman filter design using the revised reference error model placing the emphasis on a minimal state size Kalman filter mechanization.
- Review and comment on the adequacy of the TRW flight test program to appropriately test the effectiveness of the Kalman filter in the INI system.

Reference 1 is frequently cited in the present work. Whenever possible the notation used here is consistent with this reference. It is assumed that the reader is familiar with the concepts of suboptimal Kalman filter design, performance evaluation and sensitivity analysis as presented in, for example, in Ref. 2.

1.2 REPORT OVERVIEW

In Section 2 revisions to the INI reference error model are first discussed and an 18-state INI Kalman filter design is presented. Section 3 contains a detailed performance evaluation of the 18-state Kalman filter, including a comparison against the theoretically best performance of a fully optimally integrated INI system. The conventional vertical channel mechanization proposed by TRW is contrasted with Kalman processing of altimeter data and the problem of filter initialization is discussed. A component error budget is developed for the 18-state filter to determine major error sources limiting system performance and filter sensitivities to those error sources.

Section 4 contains discussion and comment on the TRW flight test program. Finally in Section 5 the results of this study are summarized and TASC's conclusions and recommendations are enumerated.

2. A REVISED INI REFERENCE ERROR MODEL AND KALMAN FILTER DESIGN

The INI reference error model, originally developed in Chapter 3 of Ref. 1, has been revised to reflect the results of the study reported therein and the availability of later and more complete information on inertial sensor and beacon errors. The 15-state INI Kalman filter first described in Ref. 1 has been augmented to an 18-state filter with further refinements in its design parameters. Both the updated INI reference error model and revised Kalman filter design model are described in this section.

2.1 AN UPDATED INI REFERENCE ERROR MODEL

The reference system error model used in the first INI Support Study was described in detail in Chapter 3 of Ref. 1. This model included beacon range and range-rate errors, baro-altimeter errors, and inertial system errors corresponding to the AN/ASN-90 Inertial Measurement Set (IMS). As a result of these studies, and in particular, the component error budget generated therein, and the recent availability of a detailed IMS error model (Ref. 3), the INI reference error model has been updated. This section describes only the changes between the reference system error models of this and the previous study.

In Table 2.1-1 the reference error model state selection used in this study is compared with that used in Ref. 1. The major differences between the two models lie in the area of inertial instrument errors.

TABLE 2.1-1

INI SYSTEM REFERENCE ERROR MODEL COMPARISONS

Error State Quantity	No. of States	No. of States	Comment
	Flight Test Support Study Model (Ref. 1)	Current INI Model	
Position	3	3	Unchanged
Velocity	3	3	Unchanged
Platform Tilt	3	3	Unchanged
Altimeter	2	2	Unchanged
Gyro Bias	3	3	Unchanged
Gyro G-Sensitive	3	3	Unchanged
Gyro Scale Factor	3	-	Deleted
Gyro Random	-	-	White Noise
Accelerometer Bias	3	3	Unchanged
Accelerometer Scale Factor	-	2	Added
Accelerometer Random	-	-	White Noise
Accelerometer Misalignment	-	3	Added
User Clock	2	2	Relative Clock
Beacon Clocks	8	6	Relative Clocks
TOTAL*	33	33	

*Total does not include random terms which were modeled as part of the system white noise vector.

Basically, the current reference error model was obtained from the earlier model by eliminating gyro torquer scale factor errors and adding accelerometer scale factor and misalignment errors.

The AN/ASN-90 Inertial Measurement Set (IMS) will be used in the INI tests. The inertial instrument error models used in our first study were transmitted to TASC verbally by the IMS vendor. For the present study a complete listing of inertial instrument error models was available (Ref. 3). The additional inertial instrument errors not included in our first INI study reference system error model are gyro input axis misalignments and accelerometer scale factor and input axis misalignments. These are all bias-type errors. If all these errors were modeled, they would add 15 more states to the INI reference error model. However as discussed below many of these errors were eliminated by appealing to physical reasoning and the error budget results of the first study.

The first INI component error budget reported in Ref. 1 showed that gyro torquer scale factor error contribution to any INI system error was insignificant ($< 1\%$). Gyro drift rate error caused by gyro input axis misalignments has the same mathematical form as the drift rate error caused by torquer scale factor errors. Furthermore since the gyro input axis misalignments are comparable in magnitude to the scale factor errors (2.9×10^{-4} vs. 3.0×10^{-4}), they will produce comparable drift rate errors. We may therefore conclude that gyro misalignments will not cause significant system errors. Neither gyro torquer scale factor nor input axis misalignment angles are included in the present INI reference system error model.

The flight profiles recommended by TRW in Ref. 7 will produce lateral accelerations of up to 0.3 g. In the presence of this acceleration, the horizontal accelerometer scale factor terms produce acceleration errors of $60 \mu\text{g}$ which are comparable to the level accelerometer null bias terms. These terms were therefore included in the INI reference error model. Since the simulated flights are at constant altitude, the

TABLE 2.1-2
BEACON/INERTIAL SYSTEM REFERENCE ERROR
MODEL STATE COMPLEMENT

STATE	SYMBOL	DESCRIPTION		RMS INITIAL VALUE
1	δR_N	North	Position Error	4000 ft
2	δR_E	East		4000 ft
3	δh	Vertical		200 ft
4	δV_N	North	Velocity Error	8 ft/sec
5	δV_E	East		8 ft/sec
6	δV_Z	Vertical		1 ft/sec
7	ϕ_N	North	Platform Tilt Error	0.3 min
8	ϕ_E	East		0.3 min
9	ϕ_Z	Vertical		3.0 min
10	δh_{A1}	Bias	Baroaltimeter	200 ft
11	δh_{A2}	Markov		33 ft
12	ϵ_{bN}	North	Gyro Drift Bias	0.01°/hr
13	ϵ_{bE}	East		0.01°/hr
14	ϵ_{bZ}	Vertical		0.02°/hr
15	ϵ_{gN}	North	Mass Unbalance Drift	0.3°/hr/g
16	ϵ_{gE}	East		0.3°/hr/g
17	ϵ_{gZ}	Vertical		0.3°/hr/g
18	μ_{gN}	North	Accelerometer Bias	75μg
19	μ_{gE}	East		75μg
20	μ_{gZ}	Vertical		106μg
21	μ_{sFN}	North	Accelerometer Scale Factor	0.02%
22	μ_{sFE}	East		0.02%
23	α_{XZ}	X about Z	Accelerometer Misalignment	0.4 mr
24	α_{ZX}	Z about X		0.4 mr
25	α_{ZY}	Z about Y		0.4 mr
26	δT_u	Phase Error	User†	10 ⁴ ft
27	$\delta \dot{T}_u$	Frequency Offset		10 ft/sec
28	δT_2	Phase Error	Beacon No. 2†	10 ⁴ ft
29	$\delta \dot{T}_2$	Frequency Offset		10 ft/sec
31	δT_3	Phase Error	Beacon No. 3†	10 ⁴ ft
31	$\delta \dot{T}_3$	Frequency Offset		10 ft/sec
32	δT_4	Phase Error	Beacon No. 4†	10 ⁴ ft
33	$\delta \dot{T}_4$	Frequency Offset		10 ft/sec

† Relative to Beacon No. 1

vertical accelerometer is sensing g only. Therefore the acceleration error induced by vertical accelerometer scale factor is a constant and indistinguishable from the vertical accelerometer null error. The rms value of the vertical accelerometer null error state has been adjusted to include the effect of vertical accelerometer scale factor error so that no additional state is required to model this error.

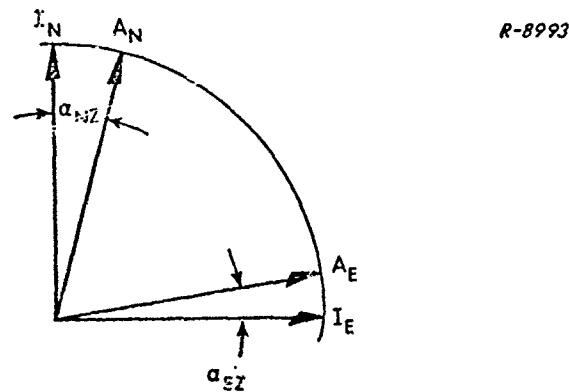
The accelerometer input axis misalignment terms are also significant. The $0.3g$ lateral acceleration acting through the stated misalignments will produce roughly $90 \mu g$ acceleration error, again comparable to the null bias errors. The number of states used to represent the accelerometer misalignments, however may be reduced from six to three.

In general six quantities are required to specify the small angle misalignments of an instrument triad relative to some nominal platform frame. However, the definition of the platform frame is somewhat arbitrary, and since we have already eliminated gyro input axis misalignment terms from our error model, it is advantageous to define the platform frame with respect to the accelerometer axes in a manner which will minimize the number of misalignment errors. Since the accelerometers are used to level the platform it is appropriate to place the platform level axes in the plane defined by the level (N, E) accelerometers. Further if the platform east axis is selected to coincide with the east accelerometer input axis only one level misalignment term remains, α'_{NZ} . Of course the vertical accelerometer misalignment errors are still present. Also, it is seen from Fig. 2.1-2 that the misalignment of the north accelerometer input axis relative to the east accelerometer input axis, α'_{NZ} , can vary in magnitude from zero to $\alpha_{NZ} + \alpha_{EZ}$. Since α_{NZ} and α_{EZ} are assumed to be independent and identically distributed we have

$$E[\alpha_{NZ}'^2] = 2E[\alpha_{NZ}^2] \quad (2.1-1)$$

where $E(\cdot)$ is the ensemble expectation operator (average value). The mean values of α'_{ZN} and α'_{ZE} must also be doubled where α'_{ZN} and α'_{ZE} are the vertical accelerometer input axes misalignments relative to the perpendicular to the plane of A_E and A_N . Thus the same total mean square misalignment error is present whether represented by three or six variables.

One more state model change deserves mention. In Section 4.2 of Ref. 1, it was shown that only the phase and frequency differences (i.e., relative phase and frequency) between beacon and user clocks was observable. The performance evaluations of Section 5 of that report further showed that only relative synchronization of user and beacon clocks was required for proper system operation. This fact was used to replace the five absolute* clock phase and frequency errors (1 user and



(I_N, I_E, I_Z) - Ideal orthogonal accelerometer set, I_Z into paper

(A_N, A_E, A_Z) - Actual accelerometer input axis orientation

Figure 2.1-2 Accelerometer Misalignments in the Plane of the Level Accelerometer Axes

*Absolute errors would be errors relative to a primary time-frequency standard, i.e., an atomic clock

4 beacons) with four relative clock error models in the primary reference system error model.

The initial value of the beacon clock frequency errors may be as large as 1 part in 10^8 rather than the value of 1 part in 10^{10} used in Ref. 1. This represents a range-rate error of 10 ft/sec and accounts for the fact that the beacon clocks may not be synchronized before each flight. As we shall see in Section 2.3, this change in initial frequency offset error will directly impact INI Kalman filter state size.

The INI Reference System error model state complement and the initial values assumed for each state in the performance evaluation to be described are listed in Table 2.1-2. A complete state space description of the INI reference error model is given in Appendix A. Changes in the vertical channel error equations which differ from the earlier study are discussed in more detail in the next paragraph.

2.2 THE VERTICAL CHANNEL MECHANIZATION

Due to the manner in which gravity is computed, the IMS vertical (altitude) channel computations are intrinsically unstable. Whenever one builds a suboptimal Kalman filter for an unstable plant, the possibility of filter divergence exists, i.e., filter estimation errors may grow arbitrarily large in time. Examples of vertical channel error divergence in a Kalman filter integrated satellite/inertial system were given in Ref. 5. It was further indicated in that reference that this divergence problem is most easily and reliably eliminated by stabilizing the vertical channel using conventional baro-altimeter damping.

TRW will mechanize a baro-altimeter damped vertical loop for the INI flight tests. The mechanization equations were originally developed by the IMS vendor and are described in Ref. 6. The mechanization to be used is shown in Fig. 2.2-1. Symbols used in the figure are defined below:

A_z = sensed vertical acceleration (specific force)

g = gravity compensation, a function of altitude and latitude

V_z = vertical velocity.

D_1 = $0.00111/\text{sec}^2$

D_2 = $0.06666/\text{sec}$

h_I = inertially derived altitude

h_A = altimeter measured altitude

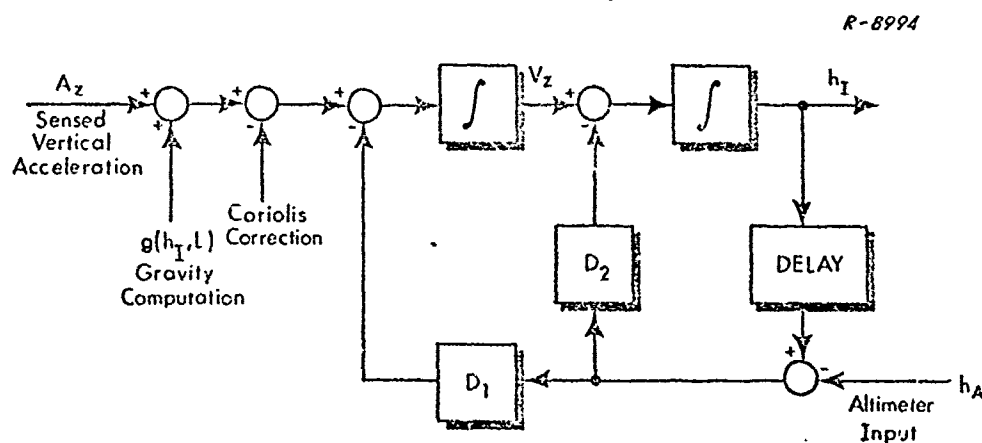


Figure 2.2-1 INI Vertical Channel Mechanization

In the mechanization, inertially derived altitude is compared with barometric altitude and the difference is fed back through appropriate gains to stabilize the loop. The constants D_1 and D_2 were selected to yield a critically damped* second order loop with a time constant, T , of thirty-two seconds. The relationship between the feedback gains and the loop time constant is

$$D_1 = \frac{1}{T^2} \quad (2.2-1)$$

$$D_2 = \frac{2}{T} \quad (2.2-2)$$

The altimeter response displays a transport lag; that is, the current output of the device is proportional to a slightly earlier value of altitude. Thus, as shown in Fig. 2.2-1, inertially indicated altitude is delayed by a similar amount before the comparison is made. This lag is typically of the order of 0.1 sec which is quite small compared to the loop time constant.

The sensed acceleration is of the form

$$A_Z = \ddot{h} - g + \text{Coriolis term} + \text{acceleration errors} \quad (2.2-3)$$

where

$$\ddot{h} = \text{2nd time derivative of altitude}$$

If the gravity compensation and Coriolis terms have been computed correctly, and if accelerometer and altimeter errors are ignored (including transport lag), the Laplace transform of inertial altitude can be written as

*A critically damped second order loop has two equal negative real roots.

$$h_I(s) = \frac{\ddot{h}(s) + (D_2 s + D_1) h(s)}{s^2 + D_2 s + D_1} \quad (2.2-4)$$

where s is Laplace transform variable. Ignoring initial conditions

$$\ddot{h}(s) = s^2 h(s) \quad (2.2-5)$$

so that Eq. (2.2-4) becomes

$$h_I(s) = \frac{s^2 h(s) + (D_2 s + D_1) h(s)}{s^2 + D_2 s + D_1} = h(s) \quad (2.2-6)$$

That is, inertially indicated altitude is equal to true altitude. Thus in the absence of errors the vertical channel mechanization is dynamically exact; that is, there are no errors due to true motion.

The error equations for the damped vertical channel are the same as those of the free inertial system, derived in Ref. 2, except for the added damping terms. These equations are presented in Appendix A. Note that the effect of transport lag has been ignored in these equations. This effect is important only during very high rates of climb or descent and has no effect on the flight profiles considered in this report. Using the system error equations, an error diagram for the vertical channel can be drawn as shown in Fig. 2.2-2. The symbols used are defined in Table 2.1-2 and Appendix A. The velocity and acceleration errors, $\delta \dot{h}_{CA}$ and $\delta \ddot{V}_{ZCA}$ respectively, are given by Eq. (2.2-6) and Eq. (2.2-7), respectively.

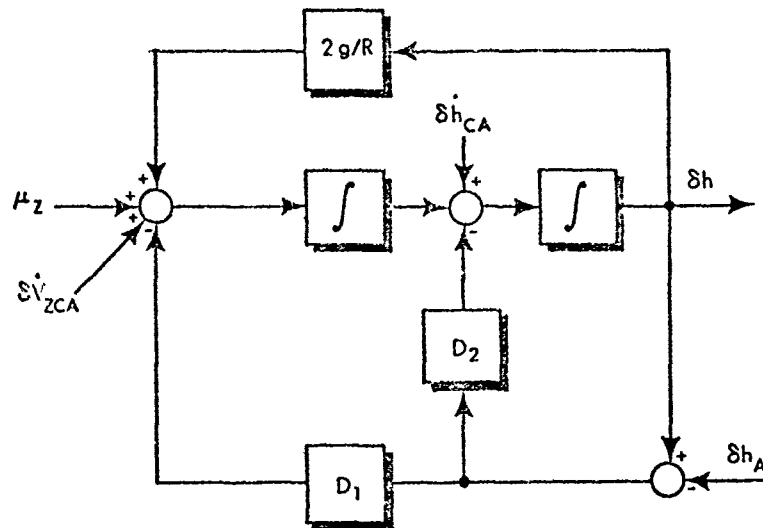


Figure 2.2-2 Vertical Channel Error Block Diagram

$$\delta \dot{h}_{CA} = \frac{V_N}{r} \delta R_N + \frac{V_E}{r} \delta R_E \quad (2.2-7)$$

$$\begin{aligned} \delta \dot{V}_{ZCA} = & -\frac{V_N}{r} \delta V_N - \left(2\Omega \cos L + \frac{V_E}{r} \right) \delta V_E \\ & + A_N \psi_E - A_E \psi_N \end{aligned} \quad (2.2-8)$$

2.3 AN 18-STATE INI KALMAN FILTER

TASC efforts in this study center on the design of a minimal state size filter for the INI System flight tests. In the design of a practical Kalman filter for any system, there is generally a minimal set of errors (i.e. states) which must be estimated if the integrated system is to remain stable and meet acceptable error performance levels. Reference 1 presented a 15-state Kalman filter design, which at that time was considered a minimal state size filter for the INI system. This minimal state selection, however, was based on the understanding that beacon clock frequencies would be synchronized to 1 part in 10^{10} or better. This represents

a range-rate error of 0.1 ft/sec or less. In light of this accurate synchronization, estimation of beacon clock drift rates was deemed unnecessary and these errors were not modeled in the 15-state filter. However, the error budget reported in Ref. 1 showed that 87% of user clock frequency error was caused by unmodeled beacon clock frequency offset. Effectively, a beacon clock frequency error translated one-for-one to a user clock frequency error. Thus if the unmodeled beacon clock frequency offsets became large, user clock synchronization with the 15-state filter would not be possible.

Subsequent to the release of Ref. 1 TRW indicated that highly accurate beacon clock synchronization measurements may not be routinely performed by the test site operators prior to each flight. Consequently, frequency differences between beacon clocks could be as large as 1 part in 10^8 , which represents an equivalent range-rate error of 10 ft/sec. With range-rate errors of this magnitude, the TRW single channel receiver will probably not acquire the beacons when operating in the narrow band aided acquisition mode. Thus the beacon relative frequency offset errors must be estimated. There are three beacon frequency offset errors relative to beacon No. 1. If these errors are added to the 15-states of the "original" INI Kalman filter, one obtains the 18-state complement used in this study.

The state vector for the INI 18-state filter design model is listed in Table 2.3-1 together with the rms initial values assumed for these errors in the performance evaluation and error budget analysis of sections 3.1 and 3.2. In addition to the nine inertial system errors, this filter estimates user and beacon clock relative phase and frequency errors and altimeter bias. If the altimeter bias were not modeled, an altitude error equal to the bias would be obtained. This error is unacceptably large (200 ft).

TABLE 2.3-1

STATE VECTOR FOR 18-STATE INI FILTER DESIGN MODEL

State	Symbol	Description	RMS Initial Value
1	δR_N^*	North	Position Error
2	δR_E^*	East	
3	δh^*	Vertical	
4	δV_N^*	North	Velocity Error
5	δV_E^*	East	
6	δV_Z^*	Vertical	
7	ϕ_N^*	North	Platform Tilts
8	ϕ_E^*	East	
9	ϕ_Z^*	Vertical	
10	δh_{A1}^*	Bias	Baroaltimeter
11	δT_u^*	Phase Error	User Clock [†]
12	$\delta \dot{T}_u^*$	Frequency Offset	
13	δT_2^*	Phase Error	Beacon [†] No. 1 Clock
14	$\delta \dot{T}_2^*$	Frequency Offset	
15	δT_3^*	Phase Error	Beacon [†] No. 2 Clock
16	$\delta \dot{T}_3^*$	Frequency Offset	
17	δT_4^*	Phase Error	Beacon No. 3 Clock
18	$\delta \dot{T}_4^*$	Frequency Offset	

[†] Relative to Beacon No. 1

In the previous study of Ref. 1 the Kalman filter processed range and range rate information and altimeter data. In the present study, however, the altimeter is used to damp the vertical channel in the conventional manner as described in the previous section. Thus the present 18-state INI filter processes beacon range and range-rate data only.

Finally, we note that all unmodeled error sources in the 18-state filter have been accounted for by additional white noise inputs to the 18-state filter design model. This is a standard approach to sub-optimal Kalman filter design which has been discussed extensively in connection with the previous satellite and beacon/inertial Kalman filter design studies of Refs. 1 and 5. A complete state-space description of the 18-state filter is given in Appendix B. A simplified diagram of the INI Kalman filter mechanization is shown in Fig. 2.3-1. In this study, it is assumed that each system state that is estimated is impulsively corrected with the negative of its estimate. This implies reset of position and velocity integrators, reset of clock phase accumulators and rapid torquing of the platform to correct tilts.

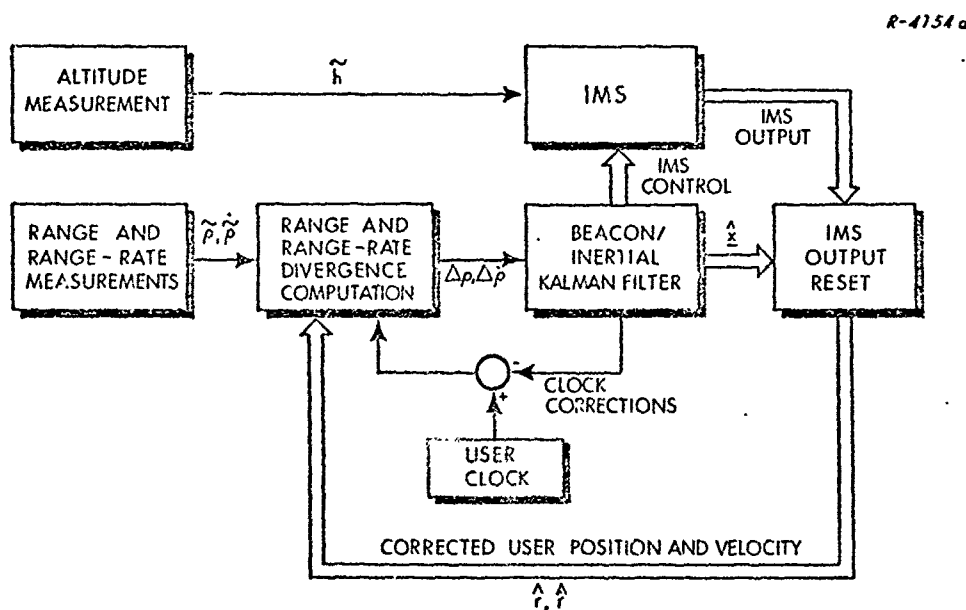


Figure 2.3-1

INI Kalman Filter Mechanization
(Conventional Vertical Channel)

3. 18-STATE BEACON/INERTIAL KALMAN FILTER PERFORMANCE EVALUATION

(U) The general strategy for Kalman filter performance evaluation is now well established. In this section the error performance of an optimally integrated INI system represented by the 33-state reference error model is first determined for a selected flight profile. The error performance of the 18-state INI Kalman filter is then predicted under the same conditions and compared against the baseline optimal results. A component error budget is next generated for the 18-state filter to isolate major integrated system error sources and determine filter sensitivity to these error sources. This section also contains a comparison of the current 18-state INI Kalman filter and the preliminary 15-state filter design reported in Ref. 1. The section ends with a discussion of the filter initialization problem. All performance predictions cited in this section were generated with the time-varying version of the covariance error analysis program described in Ref. 2.

3.1 BASELINE OPTIMAL AND 18-STATE FILTER COMPARISON

The flight profile used in the performance evaluation to be described is shown in Fig. 3.1-1. The beacon geometry is identical to that recommended and used in the studies reported in Ref. 1. The flight profile consists of three circuits over the beacon net at an altitude of 30,000 ft, and a speed of 400 ft/sec. Range and range-rate data from a single beacon are processed every six seconds. This figure represents the expected maximum time required for the beacon receiver to break lock

ACTIVE PHASE :
3 CIRCUITS OVER
BEACON NET

● BEACON LOCATIONS
ALTITUDE = 30,000 ft
VELOCITY = 400 ft/sec

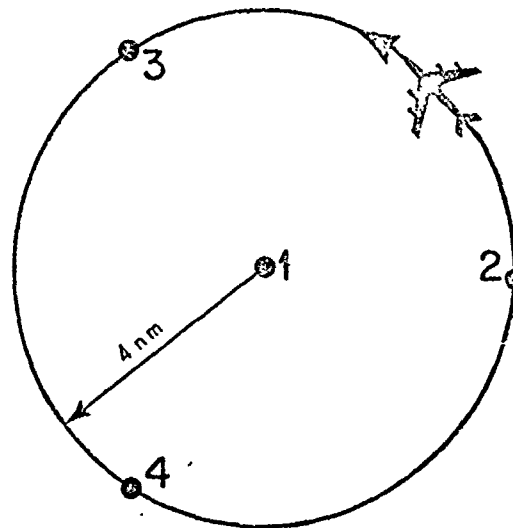


Figure 3.1-1 Beacon/Inertial Test Flight Profile

with one beacon, lock on to the next beacon and obtain the desired measurement. Beacon data is processed in a 1, 2, 3, 4 sequence beginning at $T = 6$ sec. The above profile is identical to the active phase portion of the flight profile used in Ref. 1 in order to facilitate comparisons between the two studies. Initial conditions for each of the system errors and error sources were listed in Section 2. The initial navigation errors are representative of a half-hour free inertial flight to the test area. The inertial instrument errors and clock phase and frequency errors are as described in Section 2.

(U) Plots of selected navigation errors as a function of time are shown in Fig. 3.1-2 for the optimal, and 18-state filters. Altimeter bias, and user clock relative phase and frequency errors are compared in Fig. 3.1-3. Because of the large change in most error variables over

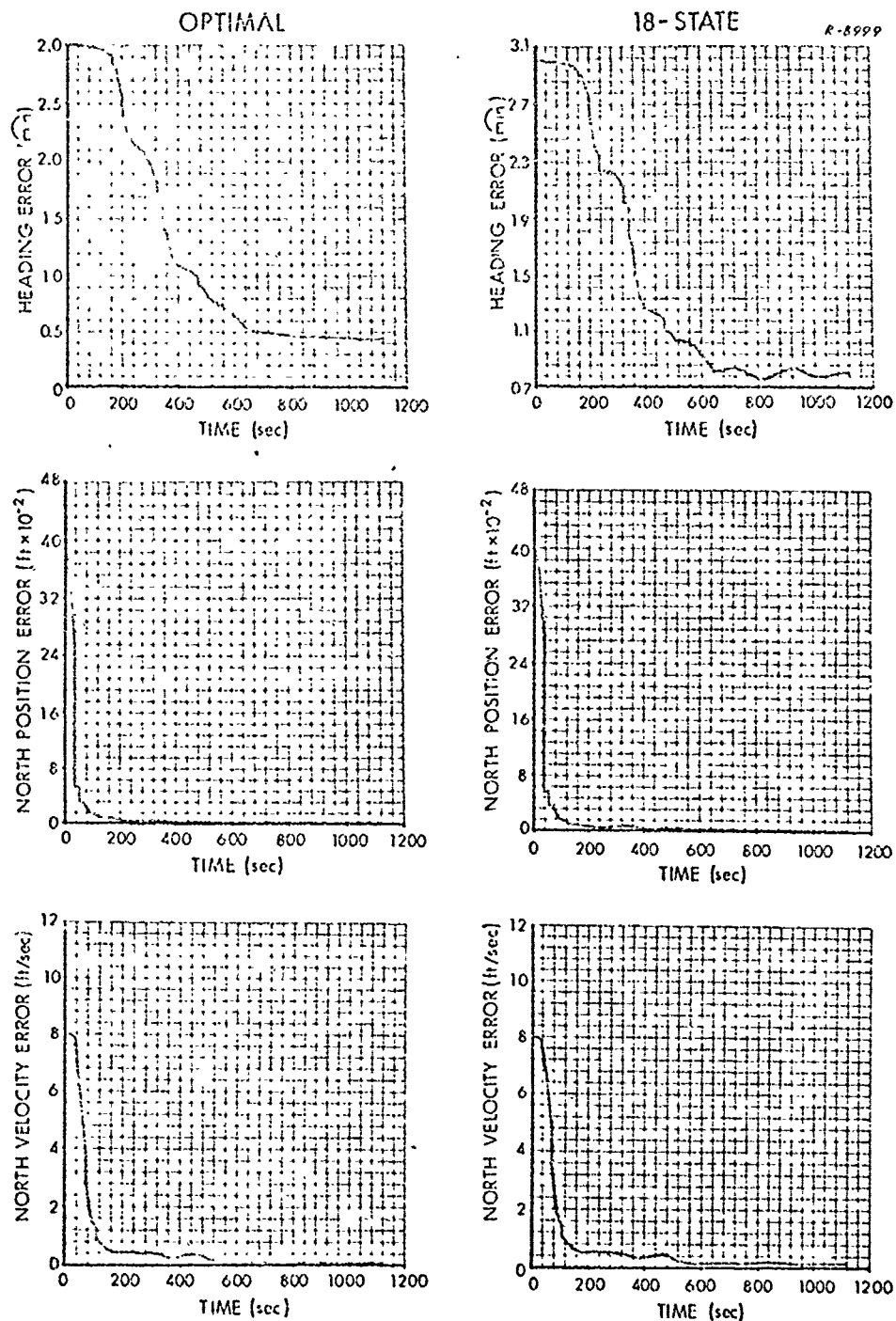


Figure 3.1-2 Comparison of rms Heading, North Position and North Velocity Errors of the Optimal and 18-State Filters

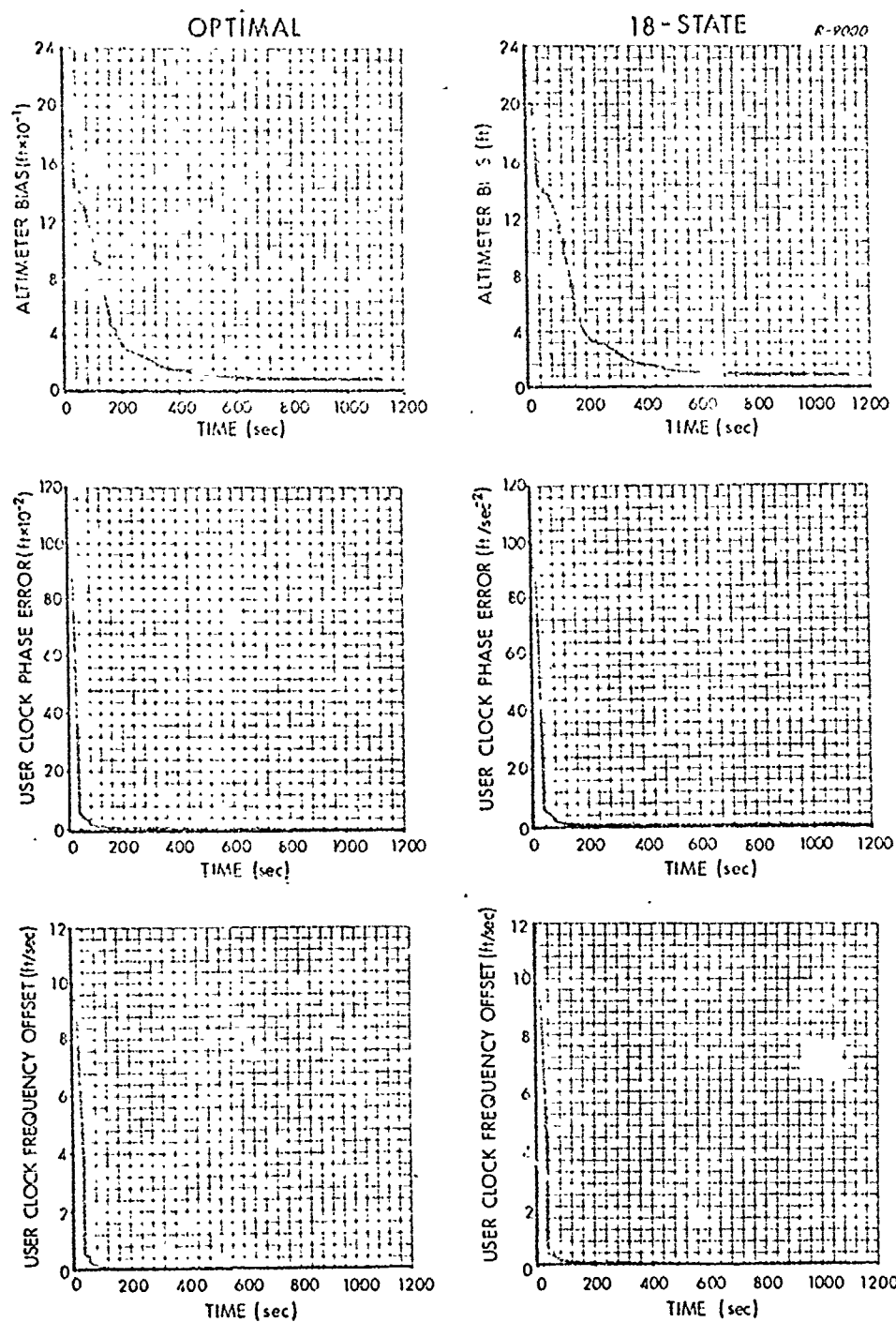


Figure 3.1-3 Comparison of rms Altimeter Bias and User Relative Clock Errors in the Optimal and 18-State Filters

the active phase, the scaling of most of these plots does not permit easy visualization of performance differences between the two filters. Note, however, that the error curves for the 18-state filter are very similar to those of the optimal filter, and that all important system error sources are bounded and near their final values within the first circuit of the simulated flight. With regard to the user clock, it is seen that the large initial drift-rate is highly observable and quickly calibrated. The major portion of user clock phase and drift-rate errors have been removed in the first third of the first circuit (120 sec).

Further comparison of the optimal and 18-state filters is most easily done in tabular form. Numerical values for the errors of interest are given in Table 3.1-1 for both filters at the end of one, two, and three circuits. Note that at all times listed the radial position error of the 18-state filter is roughly 40% above optimal. For example, at the end of three circuits the radial position errors for the optimal and 18-state filters are 17.8 ft and 25.6 ft respectively. As we shall see when the error budget is discussed, the major portion of this increase is caused by altimeter markov error which is not estimated in the 18-state filter.

With regard to radial velocity error, 18-state filter performance has stabilized out over the last circuit at approximately 0.4 ft/sec. Radial velocity error for the optimal filter averages about 0.2 ft/sec over this circuit.

At the end of three circuits, altimeter bias and user clock phase errors at 8.8 ft and 11.8 ft, respectively, are very close to the optimal altimeter bias and clock phase errors of 8.4 ft and 9.7 ft. User clock drift rate for the optimal filter at the end of 3 circuits is 0.02 ft/sec versus 0.035 ft/sec for the 18-state filter. If this latter figure is

TABLE 3.1-1

OPTIMAL AND 18-STATE FILTER PERFORMANCE COMPARISON
DURING BEACON MEASUREMENT PHASE

RMS Error	Units	T = 0	T = 360 secs		T = 720 secs		T = 1080	
		Both	Optimal	18-State	Optimal	18-State	Optimal	18-State
ϕ_z	min	3.0	1.34	1.63	0.49	0.84	0.43	0.80
δR_N	ft.	4000	35.6	56.5	12.6	17.4	9.7	15.1
δR_E		4000	27.5	40.6	9.8	14.8	8.6	13.7
δh		200	17.7	21.0	13.3	16.0	12.2	15.5
$ \delta R $	ft.	5660	48.3	72.7	20.8	27.9	17.8	25.6
δV_N	ft/sec	8.0	0.23	0.32	0.11	0.15	0.08	0.15
δV_E		8.0	0.36	0.51	0.10	0.15	0.08	0.15
δV_z		1.0	0.18	0.32	0.15	0.35	0.14	0.36
$ \delta V $	ft/sec	8.1	0.46	0.68	0.21	0.41	0.18	0.42
δh_A	ft.	200	15.9	18.1	9.3	9.7	8.4	8.8
δT_u	ft.	10^4	23.3	33.3	10.6	11.7	9.7	11.8
$\delta \dot{T}_u$	ft/sec	10	0.13	0.18	0.02	0.03	0.02	0.03

reflected through a horizontal CEP GDOP of 4* this represents a position drift rate of 0.14 ft/sec or 0.12 nm/hr. which is roughly an order of magnitude better than the basic quality of the AN/ASN-90 IMS.

Vertical channel performance deserves special mention since we have introduced conventional altimeter damping in this study. Using techniques presented in Ref. 8, it is possible to compute the steady-state

*This GDOP is typical of the simulated profile. See Section 2 of Ref. 1.

position and velocity errors of the damped vertical (DV) channel caused by altimeter bias and random errors* and accelerometer null bias errors. These errors are listed in Table 3.1-2 under the heading "DV". From the error budget studies, which are described more fully in the next section, one obtains the vertical channel response to these same error sources in the Kalman filter aided mode.

TABLE 3.1-2
COMPARISON OF STEADY STATE DAMPED VERTICAL CHANNEL
RESPONSE IN AIDED AND UNAIDED MODES
(18-STATE KALMAN FILTER)

Error Source	RMS Vertical Position Error (ft)		RMS Vertical Velocity Error (ft/sec)	
	DV	Aided DV	DV	Aided DV
Altimeter Bias	200.0	0.5	0.125	~0
Altimeter Random*	18.6	13.0	0.25	0.23
Accelerometer Bias	3.5	0.74	1.37	0.05

Notice that although the Kalman aided performance is always better than the DV performance in all error sources, the 18-state Kalman filter is most effective in reducing bias type errors. For example, in the straight DV mode, altimeter bias is by far the dominant source of altitude error. In the aided mode, however, the effect of altimeter bias is essentially removed and altimeter random error dominates. The effect of altimeter random error could be reduced by modeling the altimeter markov in the Kalman filter or by decreasing the bandwidth of the vertical channel (i.e., increasing T). However, neither approach seems warranted at this time since the altimeter random error model is not well known.

* Altimeter random errors consist of an altimeter markov error plus a white noise quantization error.

3.2 THE COMPONENT ERROR BUDGET FOR THE 18-STATE FILTER

A component error analysis is used to determine the contribution of each INI system error source to the overall error performance of the INI Kalman filter. In this manner dominant error sources are brought to light and filter sensitivity to each error source is quantified. The component error budget for the 18-state filter has been computed at the end of two circuits ($T = 720$ sec) of the active phase. At this time all navigation and clock errors have reached uniformly low levels. Thus it should be possible to determine what errors are limiting steady-state filter performance.

The component error budget immediately after a measurement is listed in Table 3.2-1. Dominant contributors to each error are boxed in the table. Histograms showing the percentage contribution of various error sources to position and velocity errors, heading error, and user clock relative phase and frequency errors are presented in Figs. 3.2-1 through 3.2-3.

According to Fig. 3.2-1, approximately 70% of the total mean square radial position error is produced by the altimeter markov error and altimeter quantization error. Measurement noise produces another 11% of the radial position error. Thus during the active phase the INI system position errors are largely a function of the external references and not strongly influenced by inertial system errors. Vertical channel and level position error histograms are also shown in Fig. 3.2-1. Altimeter random error which is not modeled in the 18-state filter is seen to produce 66% of the mean square vertical position error. This figure is consistent with the vertical channel position error budget reported in Ref. 1 for a 20-state INI Kalman filter with no random altimeter error model. Altimeter random errors also produce 75% of

TABLE 3.2-1
COMPONENT ERROR BUDGET FOR 18-STATE INI KALMAN FILTER

ERROR SOURCE	SYSTEM ERRORS											
	HEADING (min)				POSITION (ft)				VELOCITY (ft/sec)			
	rms Value		% of mse		North		East		Vertical		North	
Altimeter	0.010	—	—	—	—	—	—	—	—	—	—	—
Bias	0.236	7.9	14.9	73.4	0.06	13.1	78.5	13.0	65.9	0.070	21.6	0.076
Random												
Accelerometer												
Bias	0.045	—	0.7	—	0.6	—	—	0.7	—	0.010	—	0.016
Scale Factor	0.251	9.9	3.3	4.0	3.5	6.0	18.8	6.9	18.8	0.099	45.2	0.051
Misalignment	0.698	69.2	3.5	4.0	2.3	2.5	1.5	1.5	1.0	0.03	5.0	0.096
Gyro												
Bias	0.118	2.0	3.2	3.4	2.0	2.0	—	1.0	—	0.05	12.2	0.051
g-sensitive	0.011	—	0.5	—	0.2	—	—	0.3	—	—	—	0.002
Clocks (All)												
Phase	~0	—	~0	—	~0	—	—	~0	—	~0	—	~0
Frequency	0.023	—	3.4	3.9	1.8	1.5	—	0.6	—	0.014	1.0	0.014
Measurement Noise												
Range	0.230	7.5	5.1	8.8	3.9	7.0	5.3	5.3	10.8	0.050	12.0	0.036
Range Rate	0.064	—	2.5	2.5	2.3	2.5	2.3	2.3	2.5	0.016	1.0	0.016
Initial Conditions (Inertial)	0.156	3.5	~0	—	1.0	—	—	1.4	1.0	0.015	1.0	0.021
TOTALS	0.840	100.0	17.4	100.0	14.8	100.0	16.0	100.0	0.351	100.0	0.351	100.0

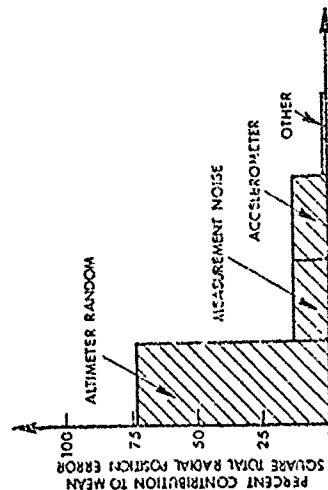
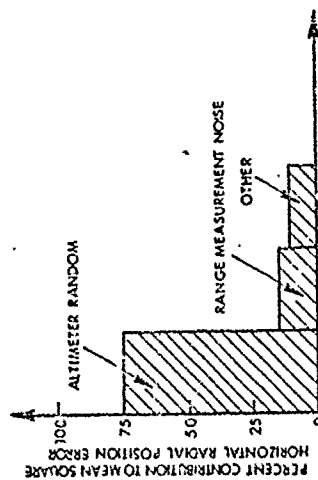
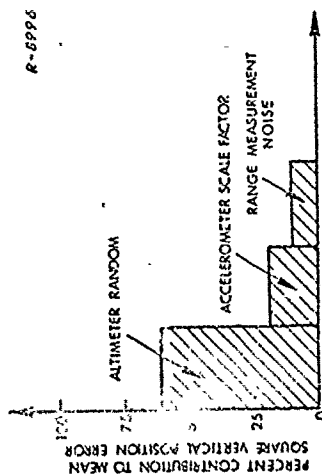


Figure 3.2-1 Position Error Budget Histograms for 18-State INI Filter (T = 720 sec)

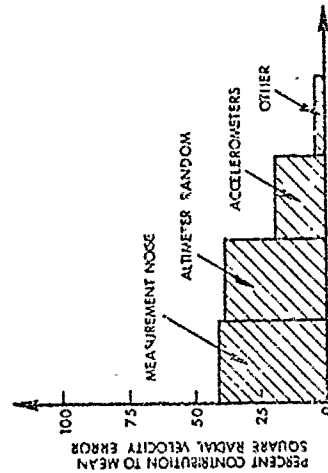
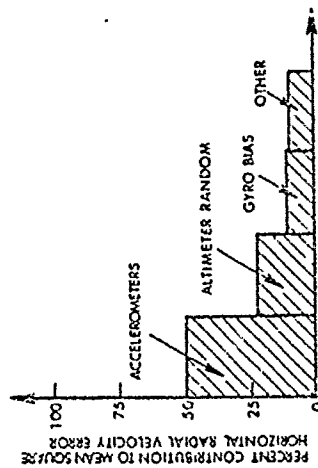
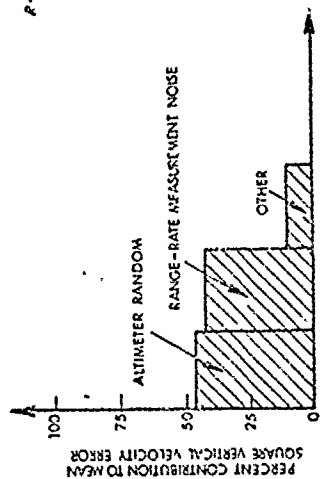


Figure 3.2-2 Velocity Error Budget Histograms for 18-State INI Kalman Filter (T = 720 sec)

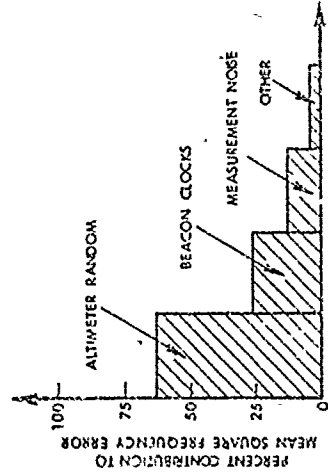
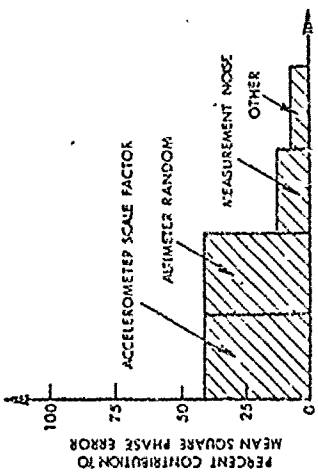
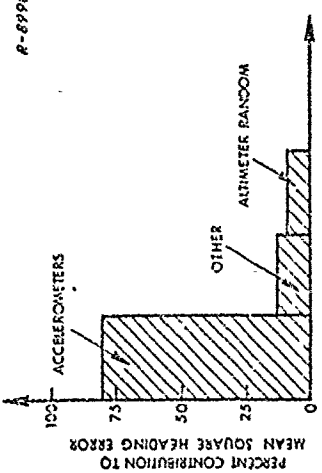


Figure 3.2-3 Heading and User-Clock Error Budget Histograms for 18-State INI Kalman Filter (T = 720 sec)

the mean square level position error. This is a direct consequence of the conventional altimeter damping of the vertical channel mechanization used in the present study. In the previous study where the altimeter was processed as a Kalman measurement, level channel accuracy was not sensitive to altimeter errors. Thus we have some measure of the price paid to stabilize the vertical channel. Note that the effect of inertial system initial conditions and user and beacon clock errors on position errors is insignificant, attesting to the high observability of these error sources.

Turning now to velocity errors, Fig. 3.2-2 shows that altimeter random error and range-rate measurement noise contribute almost equally to total radial velocity, being 37% and 34% of the total mean square error. Accelerometer scale factor and misalignment constitute the third major source with 12% of the velocity error budget. The individual vertical and horizontal velocity error histograms of Fig. 3.2-2 give a clearer picture of what is happening. From the vertical velocity histogram we see that measurement noise, and altimeter random produce most of the vertical velocity error. From Table 3.2-1 the actual percentage contributions are seen to be 46% and 42% respectively. This may be contrasted with the horizontal velocity error where accelerometer scale factor and misalignment errors cause 50% of the mean square horizontal velocity error and altimeter random errors produce another 25% of this error. Thus accelerometer scale factor and misalignment errors are the major source of horizontal velocity error and their inclusion in the INI reference error model is justified. The reason for this, of course, is largely a function of the flight profile selected. The circular flight profile produces a constant centrifugal acceleration of approximately 0.2 g in the level plane. This acceleration couples directly into the error process through the accelerometer scale factor and misalignment errors.

In an unaccelerated flight profile, these would not be significant error sources.

As shown in Fig. 3.2-3 heading error is dominated by accelerometer errors, which produce 79% of the error in this category. From table 3.2-1 it is seen that accelerometer misalignment errors cause 69% of the heading error. The dynamics of heading error recovery are discussed at length in Section 5.2 of Ref. 5. We simply note here that heading error is not directly observable from position and velocity fixes. Rather heading error is estimated by the Kalman filter from its knowledge of position and velocity errors and the inertial system dynamics which relate these errors to heading error. For example, the differential equation for north velocity error has the form

$$\delta \dot{V}_N = \frac{-g}{r} \delta R_N + \dots + A_E \phi_Z + A_E \alpha_{NE} \quad (3.2-1)$$

From this equation we see that heading error, ϕ_Z , and north accelerometer misalignment about east, α_{NE} , couple into the north velocity error equation through the common gain, A_E , which is the east component of vehicle acceleration. The 18-state filter does not model accelerometer misalignment, so that its model of north velocity error has the form

$$\delta V_N^* = \frac{-g}{r} \delta R_N^* + \dots + A_E \phi_Z^* \quad (3.2-2)$$

Now, since heading error and accelerometer misalignment affect north velocity in the same manner and since the 18-state filter does not model α_{NE} , the affect of α_{NE} on north velocity is incorrectly attributed to heading error in the 18-state filter and thus the filter misestimates ϕ_Z .

Again referring to Fig. 3.2-3 it is seen that user clock relative phase error is strongly influenced by altimeter random and accelerometer scale factor errors. Each error source produces about 40% of the total mean square user clock phase error. At first glance the accelerometer scale factor contribution to user clock phase error may appear surprising. The mechanism by which clock phase error is recovered in the INI configuration was discussed in detail in Section 2.4 Ref. 1. There it was shown that the rapidly varying geometry modulates the projection of position error into range error thus causing a spectral separation of position error and clock phase error which permits each to be estimated. Position errors are modulated cyclically with a period equal to the time of flight around the TRW profile. The position errors produced by accelerometer scale factor error, however, are also cyclic since they couple the centrifugal force vector, which is rotating in the navigation frame, into the navigation error process. The cyclic nature of accelerometer scale factor error induces a cycle position error as illustrated in Fig. 3.2-4a. When this sinusoidal position error is modulated at the same frequency by the range measurement geometry, the result is to produce a $\sin^2 \omega t$ term. But

$$\sin^2 \omega t = \frac{1}{2} - \frac{1}{2} \cos 2\omega t \quad (3.2-3)$$

so that accelerometer scale factor induced position error produces a bias and twice frequency error in range (i.e. phase). This shows up clearly in Fig. 3.2-4b which is a plot of accelerometer scale factor induced user clock phase error as a function of time.

Finally, from Fig. 3.2-3 it is seen that altimeter random error and beacon clock drift rates are the major contributors to user clock frequency error, contributing 62% and 25% respectively to this

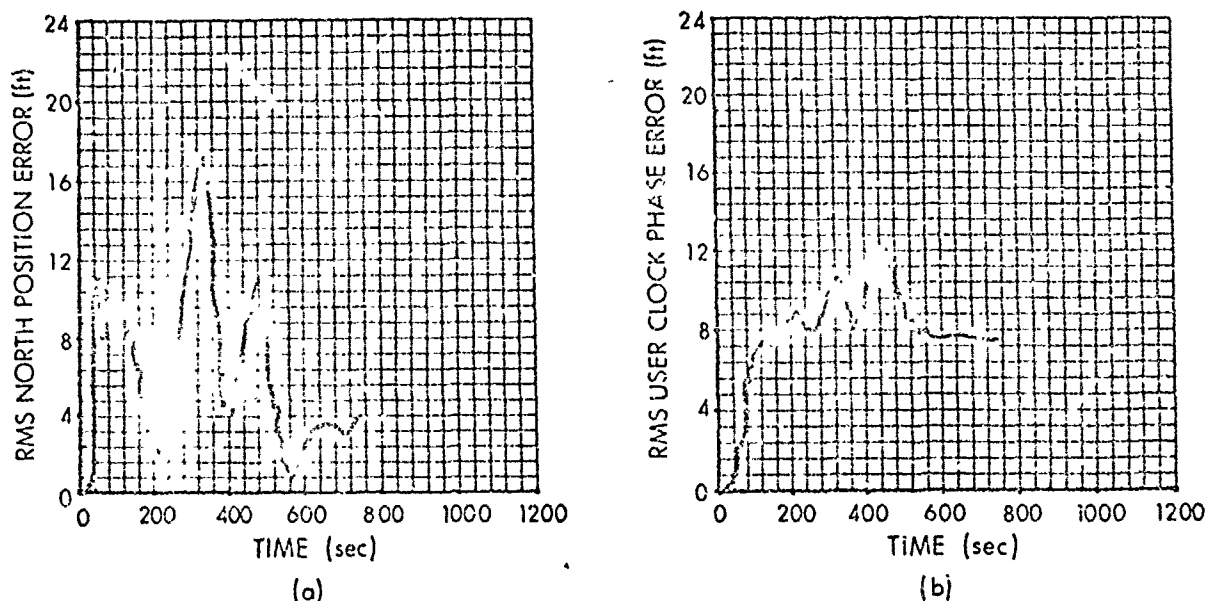


Figure 3.2-4 RMS Errors Produced by Accelerometer Scale Factor Errors

error. This should be contrasted with the previous 20-state filter study (Ref. 1) where beacon clock drift rates contributed 87% of the mean square user clock frequency error, because the 20-state filter did not estimate beacon clock drift rate.

In summary we see that error sources which are not modelled in the 18-state Kalman filter are the major contributors to all important INI system errors. Altimeter random errors and accelerometer scale factor and misalignment errors are the principle sources of error. The accelerometer errors are important because of the constant magnitude centrifugal acceleration experienced in the selected test flight profile. They would not be important in a cruise type environment.

3.3 COMPARISON OF PREVIOUS RESULTS AND CURRENT STUDIES

In this section optimal and suboptimal system performance projections for the current study are compared against similar results reported in Ref. 1. The differences between the current reference error model and the earlier reference error model were discussed in detail in Section 2. First, a conventional vertical channel damping mechanization has replaced Kalman processing of altimeter data. Secondly, accelerometer scale factor and misalignment errors have been added. Since all other conditions of the two simulations were identical, the difference in predicted performances for the two optimal systems must be caused by these model differences. Although component error budgets were not run for the optimal systems we can, with a high degree of confidence, infer the effect of the model changes on predicted optimal performance from the suboptimal error budgets.

Optimal and suboptimal system errors at the end of three circuits around the TRW flight profile are given in Table 3.3-1. Referring to the table we see that optimal radial position error and clock phase error in the current study are roughly double that predicted for the earlier 33-state model. This increase is largely attributable to the changeover from Kalman processing to conventional processing of altimeter data. Predicted optimal radial velocity error and user clock frequency error are up by approximately a factor of 3, due both to the added accelerometer errors and changed altimeter data processing. The heading error increase of some 80% is caused by accelerometer misalignments not modeled in the earlier study.

From the present discussion and the error budget study of Section 3.2 it is clear that accelerometer scale factor and misalignment errors are significant sources of error in the INI system using the TRW

profile. Their inclusion in the reference error flight model results in a more realistic prediction of baseline optimal INI system performance.

TABLE 3.3-1
COMPARISON OF CURRENT AND PREVIOUS RESULTS FOR
INI SYSTEM PERFORMANCE PREDICTIONS
(AT T = 1080 SECS)

RMS Error	Previous Study		Current Study	
	Optimal	15-State	Optimal	18-State
<u>Heading (\hat{m})</u>				
ϕ_Z	0.25	0.48	0.43	0.80
<u>Position (ft)</u>				
δR_N	4.9	18.2	9.7	15.1
δR_E	4.4	11.6	8.6	13.7
δh	5.7	12.1	12.2	15.5
$ \delta R ^*$	8.7	24.7	17.8	25.6
<u>Velocity (ft/sec)</u>				
δV_N	0.046	0.14	0.08	0.15
δV_E	0.034	0.14	0.08	0.15
δV_Z	0.030	0.16	0.14	0.36
$ \delta V ^*$	0.06	0.25	0.18	0.42
<u>Altimeter Bias (ft)</u>				
δh_{A1}	4.6	7.0	8.4	8.8
<u>User Clock</u>				
δT_u (ft)	4.6	12.1	9.7	11.8
$\delta \dot{T}_u$ (ft/sec)	0.0079	0.049	0.020	0.035

*Total radial error e.g., $|\delta R| = \sqrt{\delta R_N^2 + \delta R_E^2 + \delta h^2}$

Comparison between suboptimal filter performance predictions in the two studies can also be made. The appropriate comparison here is between the 15-state filter of Ref. 1 and the current 18-state filter, since the 18-state filter is basically the old 15-state filter with the three beacon clock relative drift-rates added. The 15/18-state filter comparison is also given in Table 3.3-1. The numerical comparison is largely self-evident, however, two points are worth noting. First, on a percentage basis the 18-state filter is much closer to its baseline optimal filter than the 15-state filter is to its 33-state optimal. Secondly, because of the addition of beacon clock drift rates to the 18-state filter, user clock errors are actually lower than those predicted for the earlier 15-state filter.

3.4 FILTER INITIALIZATION STUDIES

The performance predictions cited so far in this section were generated assuming that the initial covariance matrices for both the reference error model and the filter design model are diagonal. During the test program, however, the inertial system will have been in operation for some time prior to entry into the beacon aided mode and substantial cross-correlation between inertial system navigation errors and inertial instrument errors will undoubtedly be present. Accordingly the filter initialization studies to be described had two broad purposes. The first was to determine filter response during the active phase to more realistic reference inertial system initial conditions when using diagonal filter covariance matrix initialization. The second purpose was to determine if more realistic filter initial conditions could be obtained at entry into the active phase by starting the filter on the ground prior to take-off.

3.4.1 Initialization Study No. 1

In order to generate more realistic reference system initial conditions, a 20-minute free-inertial flight, starting from typical initial conditions produced by conventional ground alignment techniques was simulated. A northwest flight path to the test site at an altitude of 30,000 ft and velocity of 400 ft/sec was used. This trajectory was selected to approximate a flight from Holloman AFB to the WSMR test site. This simulation generated a full reference inertial system covariance matrix upon entry into the active phase over the beacon net. The scenario for the first initialization study is shown in Fig. 3.4-1. At the beginning of the active phase the filter covariance, which was diagonal, was initialized with the rms values shown in Table 3.4-1. The actual inertial system errors at this time are shown in Table 3.4-2 where the optimal and 18-state filter performances are compared for this study.

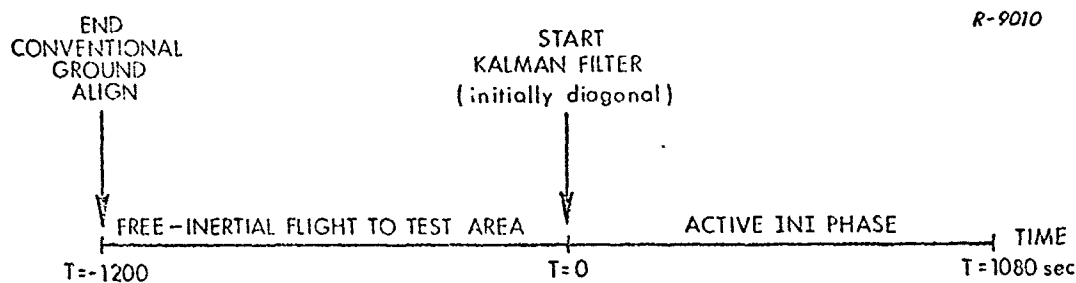


Figure 3.4-1 Scenario for Initialization Study No. 1

If the 18-state filter performance in this study is compared with results cited in Table 3.1-1 at the end of two and three circuits, they are seen to be practically identical. As indicated in Section 3.1, heading error is one of the more difficult errors to estimate so that a comparison of time histories of heading error give qualitative information on the relative performance of a given filter under varying

TABLE 3.4-1
INITIALIZATION STUDY NO. 1 RMS INITIAL VALUES FOR
18-STATE FILTER

State	Symbol	Description	RMS Initial Value
1	δR_N	North	3000 ft
2	δR_E	East	3000 ft
3	δh	Vertical	200 ft
} Position Error			
4	δV_N	North	4 ft/sec
5	δV_E	East	4 ft/sec
6	δV_Z	Vertical	0.5 ft/sec
} Velocity Error			
7	ϕ_N	North	0.4 $\widehat{\text{min}}$
8	ϕ_E	East	0.4 $\widehat{\text{min}}$
9	ϕ_Z	Vertical	3.0 $\widehat{\text{min}}$
} Platform Tilt			
10	δh_A	Altimeter Bias	200 ft
11	δT_u	Phase Error	10^4 ft
12	$\delta \dot{T}_u$	Frequency Error	10 ft/sec
} User*			
13	δT_2	Phase Error	10^4 ft
14	$\delta \dot{T}_2$	Frequency Error	10 ft/sec
} Beacon No.2*			
15	δT_3	Phase Error	10^4 ft
16	$\delta \dot{T}_3$	Frequency Error	10 ft/sec
} Beacon No.3*			
17	δT_4	Phase Error	10^4 ft
18	$\delta \dot{T}_4$	Frequency Error	10 ft/sec
} Beacon No.4*			

*Relative to Beacon No. 1

TABLE 3.4-2

INITIALIZATION STUDY NO. 1 - OPTIMAL AND 18-STATE
FILTER PERFORMANCE COMPARISON

RMS Error	Units	T = 0 sec	T = 360 sec End 1st Circuit		T = 720 sec End 2nd Circuit		T = 1080 sec End 3rd Circuit	
		System	Optimal	18-State	Optimal	18-State	Optimal	18-State
ϕ_Z	min	3.02	0.99	1.39	0.47	0.85	0.42	0.81
δR_N	ft	2270	31.1	50.2	11.1	17.5	8.9	15.1
δR_E		2244	23.9	38.8	9.5	14.8	8.3	13.7
δh		202	15.1	19.9	13.0	16.2	12.1	15.8
$ \delta R $	ft	3198	42.0	66.5	19.6	28.1	17.2	25.8
δV_N	ft/sec	3.2	0.21	0.28	0.091	0.153	0.075	0.151
δV_E		3.1	0.29	0.42	0.067	0.155	0.065	0.154
δV_Z		0.35	0.17	0.32	0.15	0.35	0.14	0.36
$ \delta V $	ft/sec	4.47	0.40	0.60	0.187	0.41	0.17	0.42
δh_A	ft	200	12.2	17.4	9.2	10.2	8.2	9.3
δT_1	ft	10^4	21.7	31.0	10.1	12.1	9.3	12.3
$\delta \dot{T}_1$	ft/sec	10	0.10	0.17	0.022	0.031	0.020	0.034

initial conditions. Heading error time histories for the 18-state filter in the baseline performance run of Section 3.1 and the present initialization study are shown in Fig. 3.4-2. Note the great similarity in these curves. The major conclusion to be drawn from this first initialization study is that the 18-state filter is largely insensitive to the presence of off-diagonal terms in the reference system initial covariance matrix. Alternately, the filter's lack of knowledge of significant initial cross-correlations in reference system errors does not materially degrade its performance.

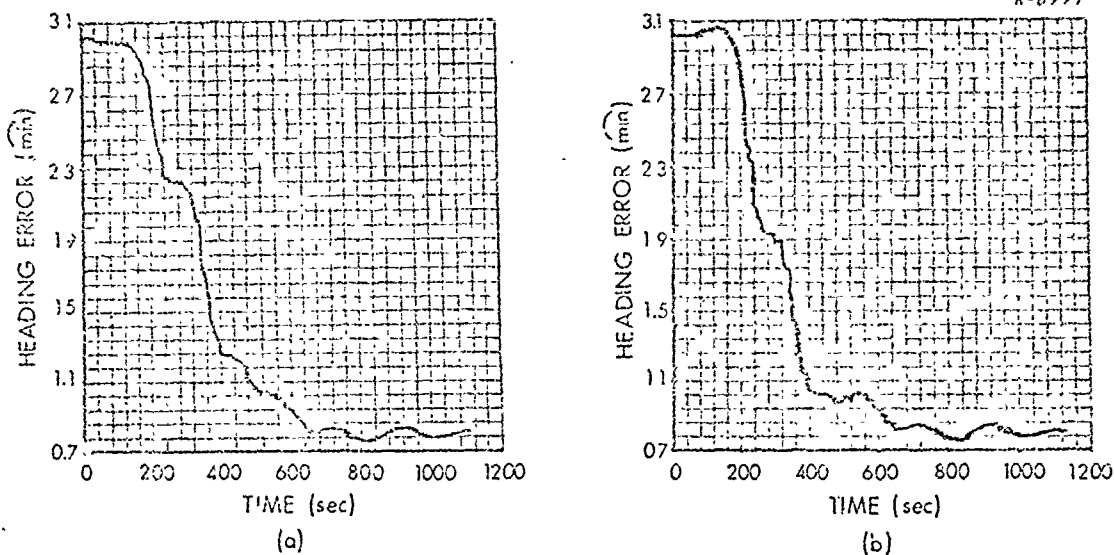


Figure 3.4-2 18-State Filter Heading Error Time Histories for the Baseline Run Initialization Study No. 1(b)

3.4.2 Initialization Study No. 2

If the errors of the optimal filters in the baseline performance evaluation of Section 3.1 and the first initialization study are compared, it is seen that the latter are generally smaller. In particular, heading error at the end of one circuit is much smaller in the first initialization study (0.99 min vs 1.34 min). Thus it appears that cross-correlation between various system errors when present and known to the filter can result in improved transient performance and somewhat lower steady-state errors. The second initialization study was made to determine whether or not the 18-state filter could be made to generate the appropriate cross-correlations in its covariance computations. In order to do this, filter estimates of system errors must be strongly correlated with actual system errors at some previous time (i. e., the filter must update the system with external data). This was accomplished by simulating a Kalman ground align mode. In this mode the aircraft remains stationary at a known point. The Kalman filter is configured to accept position and velocity fixes corresponding to this known point and zero velocity. The Kalman filter is then used to predict inertial system error build-up during the flight to the beacon net.

In this study a 10-min ground align was first simulated. Position was assumed to be known to within a bias of 10 ft per axis although this bias was not modeled in the 18-state filter. An rms velocity measurement error of 0.2 ft/sec was also assumed to account for wind gusts and aircraft loading effects. Velocity and position fixes were processed every 6 seconds. The scenario for the second initialization study is shown in Fig. 3.4-3.

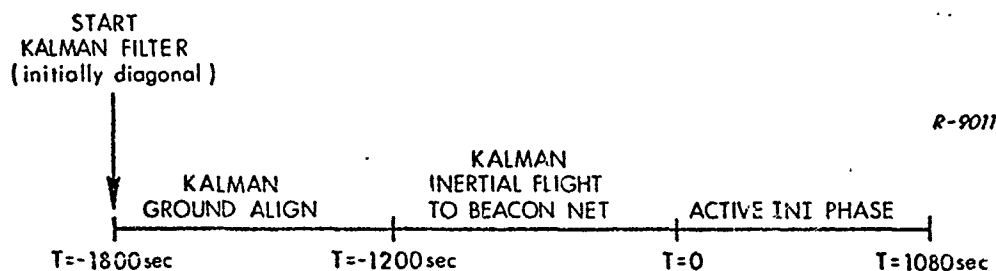


Figure 3.4-3 Scenario for Initialization Study No. 2

Optimal and 18-state filter performance in the second initialization study is summarized in Table 3.4-3. During the active phase optimal filter errors in all categories are somewhat lower than those in any of the earlier simulations. The 18-state filter error performance, however, at the end of 3 circuits over the beacon net is essentially the same as before, with the exception of heading error which is actually somewhat worse than in the first study, i.e., 0.93° min vs 0.81° min.

It is very difficult to isolate the exact cause for this small increase in heading error without additional analysis. However, some general observations can be made. Looking back to the end of ground align it is seen that 18-state filter errors are very close to optimal. This is so because errors in both the optimal and suboptimal filters at this time are largely controlled by the external velocity and position information which is very accurate. At the end of the 20-min flight to the test area, however, 18-state filter radial position error at 1054 ft is some

TABLE 3.4-3

FILTER INITIALIZATION STUDY NO. 2 - OPTIMAL AND 18-STATE FILTER
PERFORMANCE COMPARISON

Error State	Units	T = -1200 sec End Ground Align		T = 0 Enter Beacor Net		T = 360 secs		T = 720 secs		T = 1080 secs	
		Optimal	18-State	Optimal	18-State	Optimal	18-State	Optimal	18-State	Optimal	18-State
ϕ_Z	$\widehat{\text{min}}$	2.04	2.50	2.10	2.59	0.68	1.55	0.38	1.00	0.30	0.93
δP_N		9.9	10.0	123	786	19.8	53.5	10.8	17.9	8.6	15.1
δP_E	ft	9.9	10.0	128	702	14.9	40.6	9.2	15.8	7.7	14.6
δh		10.5	10.5	21.6	21.6	12.8	16.3	10.8	15.1	10.0	14.9
$ \delta R $		17.5	17.6	179	1054	27.9	69.1	17.8	28.2	15.3	25.3
δV_N		0.002	0.004	0.25	1.48	0.10	0.29	0.074	0.15	0.061	0.14
δV_E	ft/sec	0.002	0.004	0.26	1.33	0.16	0.49	0.061	0.21	0.051	0.19
δV_Z		0.204	0.206	0.35	0.35	0.17	0.31	0.15	0.37	0.14	0.37
$ \delta V $		0.20	0.21	0.50	2.00	0.25	0.65	0.18	0.45	0.16	0.44
δh_A	ft	9.9	10.0	9.9	10.0	7.5	8.1	5.9	7.4	5.1	7.3
δT_1	ft	--	--	10^4	10^4	15.2	33.7	7.5	11.6	6.5	11.5
$\delta \dot{T}_1$	ft/sec	--	--	100	100	0.63	0.17	0.022	0.033	0.020	0.035

6 times worse than optimal. This result is perhaps not unexpected since the 18-state filter was optimized for processing beacon data at a high rate and not for long-term extrapolation of inertial system errors. The covariance matrix computed by the 18-state filter at this time not only underestimates the true rms value of all system errors but also errs in the ratio of these errors. For example, true rms north and east position errors shown in Table 3.4-3 at $T = 0$ are roughly equal at 786 and 702 ft, respectively. However, the 18-state filter covariance computation places the rms north and east position errors at this time at 770 and 493 ft, respectively. Similar errors in magnitude and ratio are present in the velocity and tilt angle covariances. This suggests that the unmodeled errors cause the covariance matrix computed in the 18-state filter algorithm over the 20-min Kalman inertial flight to be incorrect not only in rms value but also in important off-diagonal terms, which may account for the increased heading error.

In terms of final system accuracy at the end 3 circuits over the beacon net, there appears to be no advantage to mechanizing a Kalman ground align mode. However, with ground-align, 18-state filter errors are substantially lower upon entry into the beacon net than those predicted for the free-inertial flight to the test area. This latter fact may be significant in reducing time required to put the receiver into its aided acquisition mode and in reducing nonlinear measurement effects peculiar to the short baseline beacon geometry (as opposed to operational satellite deployment) as discussed in Ref. 4.

3.5 PERFORMANCE EVALUATION SUMMARY

The performance evaluations reported in this section indicate that an 18-state INI Kalman filter mechanization can provide navigation

accuracies consistent with the INI test objectives. In particular, these studies show that highly accurate pre-flight synchronization of beacon clocks is not required and that the 18-state filter is relatively insensitive to initial condition uncertainties in general.

The vertical channel mechanization proposed by TRW should produce acceptable vertical channel accuracy while greatly reducing the possibility of Kalman filter divergence. The error budget studies have shown, however, that unmodeled system error sources, and in particular altimeter and accelerometer errors, are major contributors to navigation errors with the 18-state filter mechanization. Thus in any move to increase filter state size, inclusion of these errors should be considered.

4.

TRW INI TEST PLAN REVIEW

(I) The INI flight test objectives are described in Section 2 of Ref. 4 and the general test plan is contained in Ref. 7. The major objective of the test program is to demonstrate that a single channel receiver can sequentially acquire signals from a set of beacons under computer control using filtered inertial system data. Additional objectives are the evaluation of integrated system accuracy and software (Kalman filter, receiver aiding algorithms, etc.) performance.

(II) As part of the study effort described herein, TASC undertook a review of the TRW INI test program. This review was directed primarily toward the unique problems which arise in the testing of Kalman filter integrated systems. More specifically the review was aimed at ascertaining whether adequate data are being taken for both in-flight and post-flight filter evaluation and trouble shooting and whether appropriate filter diagnostic procedures are available to pinpoint filter deficiencies and incorporate appropriate design changes into the test program.

A brief description of the flight instrumentation will aide in understanding the TASC comments. The flight instrumentation consists of real-time (or near real time) displays and a tape recorder. The real time displays include a control and display unit, an analog strip chart recorder and a printer. The real time displays monitor system status and performance and are intended to give the operator data to assess the progress of the test, alter the flight test plan, adjust and/or repair equipment, and make unscheduled inputs to the flight program. The tape recorder is intended to record sufficient data for post-flight analysis and reconstruction.

The TRW approach to flight data recording is basically to obtain sufficient data to assess INI system accuracy, reconstruct the flight trajectory, and to "refly" the Kalman filter in a ground-based interpretative computer simulation. Thus there is no exhaustive, step-by-step recording of program variables in each computation cycle. Typical of the data to be recorded are

- receiver input/output words
- altimeter data
- IMU accelerometer outputs
- IMU gyro torquing signals
- IMU gimbal angles
- IMU/INI misalignment angles
- INI Navigation outputs
- IMU Navigation outputs
- Kalman state vector
- Kalman filter covariance matrix diagonal elements
- Time

The real-time display consists of a Control and Display unit, an analog strip chart recorder, and a printer. The printer outputs essentially the same kind of data as listed above and is the primary source of information for in-flight assessment of system performance.

TASC has reviewed the INI general test plan (Ref. 7) and offers the following over-all comments:

- The flight profiles and flight-test sequence recommended by TRW appear consistent with the flight-test objectives.

- Sufficient data are being recorded for proper post-flight evaluation in accordance with the TRW philosophy cited above.
- In-flight data displays to the operator are not of a form which best permits rapid and direct assessment of filter performance.

The last comment requires additional amplification. In order to achieve the primary test objective of successful receiver operation in the inertially aided mode, the Kalman filter must converge. The only direct measure of Kalman filter convergence available in real-time is the measurement residuals, specifically the range and range-rate divergences. Recall from Section 2 of Ref. 1 that these quantities are the difference between measured range (range-rate) and range (range-rate) computed (i.e. estimated) from INI navigation quantities. If the Kalman filter has converged these differences will be consistently "small" in some statistical sense. If these differences are not "small" corrective action can be initiated by the operator. Such action could include filter reinitialization.

The data called out in Ref. 7 for printer display does not directly measure filter convergence. For example both free inertial* and integrated NAVSAT/inertial position and velocity are printed. However, one would not expect these two sets of variables to agree, except in some gross sense. Thus differences in these quantities do not necessarily imply poor filter performance. We note that the display of selected Kalman measurement residuals is suggested in Ref. 4, yet they are absent from the printer variable list given in Ref. 7.

*Both the aided and free-inertial navigation solution are computed in flight.

SUMMARY AND RECOMMENDATIONS

In the first portion of this study a revised INI error model was developed. The major changes in this model were the addition of accelerometer scale factor and misalignment errors, the switch to conventional barometric altimeter damping of the vertical channel mechanization, and the use of coarsely synchronized beacon clocks. The change from accurate to coarse beacon clock synchronization made it necessary to estimate beacon clock drift rates in the INI Kalman filter. This required the addition of three states to the 15-state Kalman filter mechanization described in Ref. 1. A performance evaluation of the resulting 18-state filter, including a comparison against a fully optimally integrated INI system was then reported. The results of this evaluation may be summarized as follows:

- Predicted baseline optimal navigation errors with the revised INI reference error model are roughly a factor of two larger than the original predictions made by TASC in Ref. 1. For example, predicted rms radial position error has increased from 8.7 ft to 17.8 ft.
- Projected navigation performance of the 18-state INI Kalman filter is acceptable and consistent with the INI test objectives.
- Altimeter random errors and accelerometer scale factor and misalignment errors are the major sources of system error in the flight profiles studied. These errors are not modelled in the 18-state filter.
- The conventional vertical channel mechanization proposed by TRW is satisfactory, it provides the required vertical channel stabilization at the

expense of somewhat greater system sensitivity to altimeter random errors than Kalman processing of altimeter data.

- The 18-state filter is relatively insensitive to initial condition uncertainties.

The study then turned to a discussion of the TRW test program, with special emphasis on the Kalman filter related portions of the tests. It was generally concluded that the flight test profiles, and flight data recording were appropriate to the flight test objectives. However, it was felt that the in-flight displays to the operator were not the most appropriate for rapid assessment of proper Kalman filter operation.

Based upon the studies summarized above the following recommendations are offered:

- Mechanize an 18-state INI Kalman filter for use in the initial aided flights.
- Provide real-time display of selected Kalman filter measurement residuals and statistical evaluation of these residuals as discussed in Section 4, to permit rapid evaluation of filter convergence and/or appropriate in-flight corrective action.

APPENDIX A
STATE SPACE SPECIFICATION OF THE
INI REFERENCE ERROR MODEL

A.1 INTRODUCTION

In order to use the covariance equations of error analysis developed in Ref. 2, the reference system error equations must be written in vector-matrix or state-space form. These equations are specified by the following reference system elements:

- \underline{x} = state vector
- F = dynamics matrix
- Q = system noise covariance matrix
- P_0 = initial condition matrix
- H_{ρ} = range measurement matrix
- R_{ρ} = range measurement noise covariance matrix
- $H_{\dot{\rho}}$ = range-rate measurement matrix
- $R_{\dot{\rho}}$ = range-rate measurement noise covariance matrix

The 33 components of the INI system reference error model state vector and their initial values were defined in Table 2.1-2. The remaining matrices which define this model are presented in this appendix.

A.2 REFERENCE SYSTEM F AND Q MATRICES

The reference system F matrix, in partitioned form, is given below:

$$F = \begin{matrix} & \begin{matrix} 1-9 & 10-11 & 12-17 & 18-25 & 26-33^* \end{matrix} \\ \begin{bmatrix} F_{11} & F_{12} & F_{13} & F_{14} & 0 \\ 0 & F_{22} & 0 & 0 & 0 \\ 0 & 0 & 0 & 0 & 0 \\ 0 & 0 & 0 & 0 & 0 \\ 0 & 0 & 0 & 0 & F_{55} \end{bmatrix} & \end{matrix} \quad (A.2-1)$$

*Numbers indicate columns occupied by each partition. Refer to Table 2.1-2 for definition of state vector elements.

In the above equation F_{11} is the 9×9 dynamics matrix of inertial system errors. Similarly, F_{22} describes the baro-altimeter error dynamics and F_{55} the user and beacon clock error dynamics. The gyro and accelerometer error states are characterized as biases and therefore have zero self-coupling as illustrated in Eq. (A.2-1). Matrices F_{12} , F_{13} and F_{14} provide for the coupling of the baro altimeter, and gyro and accelerometer errors into the inertial system error states. These submatrices are specified in Eqs. (A.2-2) through (A.2-6).

$$F_{11} =$$

$$\begin{bmatrix} 0 & -\frac{V_E}{r} \tan L & -\frac{V_N}{r} & 1 & 0 & 0 & 0 & 0 & 0 \\ \frac{V_E}{r} \tan L & 0 & -\frac{V_E}{r} & 0 & 1 & 0 & 0 & 0 & 0 \\ \frac{V_N}{r} & \frac{V_E}{r} & -D_2 & 0 & 0 & -1 & 0 & 0 & 0 \\ -\left(\frac{A_z}{r} + g\right) & \frac{A_E \tan L}{r} & 0 & 0 & -\left(\frac{2\Omega \sin L}{r} + \frac{V_E \tan L}{r}\right) & \frac{V_N}{r} & 0 & -A_z & A_E \\ 0 & -\left(\frac{A_z + A_N \tan L + g}{r}\right) & 0 & \left(\frac{2\Omega \sin L}{r} + \frac{V_E \tan L}{r}\right) & 0 & \left(\frac{2\Omega \cos L}{r} + \frac{V_E}{r}\right) & A_z & 0 & -A_N \\ \frac{A_N}{r} & \frac{A_E}{r} & \frac{-2z}{r} + D_1 & -\frac{V_N}{r} & -\left(\frac{2\Omega \cos L}{r} + \frac{V_E}{r}\right) & 0 & -A_E & A_N & 0 \\ -\frac{\Omega \sin L}{r} & \left(\frac{V_N \tan L}{r} + \frac{V_Z}{r^2}\right) & -\frac{V_E}{r^2} & 0 & \frac{1}{r} & 0 & 0 & \left(\frac{\Omega \sin L}{r} + \frac{V_E \tan L}{r}\right) \frac{V_N}{r} \\ -\frac{V_Z}{r^2} & \frac{V_E \tan L}{r} & \frac{V_N}{r^2} & -\frac{1}{r} & 0 & 0 & \left(\frac{\Omega \sin L}{r} + \frac{V_E \tan L}{r}\right) & 0 & \left(\frac{\Omega \cos L}{r} + \frac{V_E}{r}\right) \\ -\left(\frac{\Omega \cos L}{r} + \frac{V_E}{r^2} \sin^2 L\right) & -\frac{\tan L}{r^2} (V_N \tan L + V_Z) & 0 & 0 & -\frac{\tan L}{r} & 0 & -\frac{V_N}{r} & -\left(\frac{\Omega \cos L}{r} + \frac{V_E}{r}\right) & 0 \end{bmatrix}$$

(A.2-2)

where

$$r = R_e + h$$

$$R_e = \text{earth's radius}$$

$$V_N = \text{north component of velocity}$$

$$V_E = \text{east component of velocity}$$

$$V_Z = \text{vertical component of velocity}$$

$$g = \text{gravity}$$

$$\Omega = \text{earth rate}$$

$$L = \text{vehicle latitude}$$

$$A_N = \text{north component of specific force}$$

$$A_E = \text{east component of specific force}$$

$$A_Z = \text{vertical component of specific force}$$

$$F_{22} = \begin{bmatrix} 0 & 0 \\ 0 & -\beta_A \end{bmatrix} \quad (\text{A. 2-3})$$

where β_A = altimeter Markov inverse correlation time.

$$F_{55} = \begin{bmatrix} 0 & 1 & 0 & 0 & 0 \\ 0 & 0 & 0 & 0 & 0 \\ 0 & 0 & 1 & 0 & 0 \\ 0 & 0 & 0 & 1 & 0 \\ 0 & 0 & 0 & 0 & 1 \end{bmatrix} \quad (\text{A. 2-4})$$

$$F_{12} = \begin{bmatrix} 0 & 0 \\ 0 & 0 \\ +D_2 & +D_2 \\ 0 & 0 \\ 0 & 0 \\ +D_1 & +D_1 \\ 0 & 0 \\ 0 & 0 \\ 0 & 0 \end{bmatrix} \quad (\text{A. 2-5})$$

$$F_{13} = \begin{bmatrix} 0 & 0 \\ 0 & 0 \\ 1 & 0 & 0 & A_N & 0 & 0 \\ 0 & 1 & 0 & 0 & A_E & 0 \\ 0 & 0 & 1 & 0 & 0 & A_Z \end{bmatrix} \quad (\text{A. 2-6})$$

The reference system Q matrix contains the spectral levels of the white noise inputs to the various system error states. The partitioned form of the Q matrix is given as follows

$$Q = \begin{array}{c|c|c|c|c} & 1-9 & 10-11 & 12-17 & 18-25 & 26-33 \\ \hline Q_{11} & 0 & 0 & 0 & 0 \\ 0 & Q_{22} & 0 & 0 & 0 \\ 0 & 0 & 0 & 0 & 0 \\ 0 & 0 & 0 & 0 & 0 \\ 0 & 0 & 0 & 0 & Q_{55} \end{array} \quad (A.2-7)$$

and the submatrices are given below.

$$Q_{11} = \begin{array}{c|cc|ccc} & & & & & & \\ \hline & 0 & & 0 & & & 0 \\ \hline & 0 & q_4 & 0 & 0 & & 0 \\ & & 0 & q_5 & 0 & & \\ & & 0 & 0 & q_6 & & \\ \hline & 0 & & 0 & & q_7 & 0 & 0 \\ & & & & & 0 & q_8 & 0 \\ & & & & & 0 & 0 & q_9 \end{array} \quad (A.2-8)$$

where

$$q_i = 2\sigma_i^2 T_i \quad i = 4, 5, 6, 7, 8, 9 \quad (A.2-9)$$

and

σ_i^2 = variance of Markov noise

T_i = correlation time of Markov process

The system noises defined in Eq. (A.2-8) represent accelerometer (4, 5, 6) and gyro (7, 8, 9) errors whose bandwidth is greater than the system bandwidth and can be approximated with white noise of spectral level given by Eq. (A.2-9). The system noise covariance associated with the baroaltimeter is given by

$$Q_{22} = \begin{bmatrix} 0 & 0 \\ 0 & 2\sigma_A^2\beta_A \end{bmatrix} \quad (A.2-10)$$

where

$$\sigma_A^2 = \text{altimeter Markov error variance}$$
 β_A = altimeter Markov inverse correlation time

The final submatrix of \mathbf{Q} is associated with the user and beacon clocks and is specified by the following expression

$$Q_{55} = \begin{bmatrix} q_{26} & 0 & & \\ 0 & q_{27} & & \\ & & q_{28} & 0 \\ & & 0 & 0 \\ & & & q_{30} & 0 \\ & & & 0 & 0 \\ & & & & q_{32} & 0 \\ & & & & 0 & 0 \end{bmatrix} \quad (A.2-11)$$

where q_i , ($i = 26, 28, 30, 32$) is the white noise input to each clock phase integrator. The values for these white noises are given below

$$\begin{aligned} q_{26} &= 0.02 \text{ ft}^2/\text{sec} \\ q_{27} &= 10^{-6} \text{ ft}^2/\text{sec}^3 \end{aligned} \quad (\text{A.2-12})$$

$$q_{28} = 2.0 \times 10^{-4} \text{ ft}^2/\text{sec}$$

$$q_{30} = q_{32} = q_{28}$$

A.3 REFERENCE SYSTEM H AND R MATRICES

Application of the Kalman algorithm to evaluation of the INI system requires definition of both the measurement matrix, H , and measurement noise covariance matrix, R , associated with each measurement. This measurement has the general form

$$\underline{z}_n = H_n \underline{x}_n + \underline{v}_n \quad (\text{A.3-1})$$

where

\underline{z}_n = the measurement vector under consideration at time t_n

H = the matrix describing the linear combination of state variables which comprise \underline{z}_n

\underline{v}_n = a vector of zero mean white noise with covariance R_n at t_n , i.e., $R_n = E[\underline{v}_n \underline{v}_n^T]$

The measurements in this system consist of range divergence and range-rate divergence to each beacon. These equations were specified in Section 3 of Ref. 1. They are repeated below for completeness.

The range divergence can be written as

$$\Delta \rho_i = H_{\rho_i} \underline{x} + \underline{v}_{\rho_i} \quad (\text{A.3-2})$$

where

$$R_{\rho_i} = E[v_{\rho_i}^2] \quad (A.3-3)$$

and the subscript i represents the i^{th} beacon. Expressing the unit vector between user and i^{th} beacon as

$$\frac{1}{\rho_i} = \begin{bmatrix} \gamma_{Ni} \\ \gamma_{Ei} \\ \gamma_{Zi} \end{bmatrix}, \quad i = 1, 2, 3, 4 \quad (A.3-4)$$

The matrixes H_{ρ_i} and R_{ρ_i} can be written as follows;

$$H_{\rho_1} = \begin{bmatrix} 1 & 3 & 4 & 25 & 26 & 33 \\ \gamma_{N1} & \gamma_{E1} & \gamma_{Z1} & 0 & \dots & 0 & 1 & \dots & \dots & 0 \end{bmatrix}$$

$$H_{\rho_i} = \begin{bmatrix} 1 & 3 & 4 & 25 & 26 & 24 + 2i \\ \gamma_{Ni} & \gamma_{Ei} & \gamma_{Zi} & 0 & \dots & 0 & 1 & 0 & \dots & -1 & 0 & \dots \end{bmatrix}; i = 2, 3, 4$$

$$R_{\rho_i} = \sigma_{\rho_i}^2 \quad (A.3-5)$$

The general expression for the range-rate divergence is given as

$$\Delta \dot{\rho} = H_{\rho_i} \dot{x} + v_{\rho_i} \quad (A.3-6)$$

where

$$R_{\rho_i} = E[v_{\rho_i}^2] \quad (A.3-7)$$

Using Eq. (3.1-2) of Ref. 1 the matrices H_{ρ_i} and R_{ρ_i} are readily formed as

$$\begin{aligned}
H_{\dot{\rho}_1} &= \begin{bmatrix} e_{N1} & e_{E1} & e_{Z1} & \gamma_{N1} & \gamma_{E1} & \gamma_{Z1} & \begin{matrix} 7 & 26 & 27 & 33 \\ 0 & . & . & 0 \end{matrix} & \begin{matrix} 1 & . & . & 0 \end{matrix} \end{bmatrix} \\
H_{\dot{\rho}_i} &= \begin{bmatrix} 1 & & & & & & \begin{matrix} 26 & 27 & 25+2i \\ 0 & . & 0 \end{matrix} & \begin{matrix} 1 & 0 & . & -1 & 0 & . & . \end{matrix} \end{bmatrix}; i=2, 3, 4
\end{aligned}
\tag{A.3-8}$$

and

$$R_{\dot{\rho}_i} = \sigma_{\dot{\rho}_i}^2 \tag{A.3-9}$$

The first three elements in the matrix $H_{\dot{\rho}}$ were defined as the vector of position-to-velocity error influence coefficients in Section 3 of Ref. (1).

These values are specified by the following relationship, derived in Ref. 5:

$$e_i = \frac{\dot{\rho}_i}{\rho_i} - \frac{\frac{1}{\rho_i} \cdot \dot{\rho}_i}{\rho_i} \frac{1}{\rho_i} \tag{A.3-10}$$

APPENDIX B

SPECIFICATION OF THE 18-STATE INI KALMAN FILTER DESIGN MODEL

B.1 INTRODUCTION

A filter design model is specified by a set of elements analogous to those used to specify the reference error model. Thus, one must specify the filter design model state vector, a design model dynamics matrix, noise matrix, initial condition matrix, etc. Adopting the notation of Ref. 2, the design model elements will be differentiated from the reference or "real world" elements through the use of a superscript (*) notation. Accordingly, the filter design is specified by the following elements:

\underline{x}^* = the design model state vector

F^* = the design model dynamics matrix

Q^* = the design model noise covariance matrix

P_0^* = the design model initial covariance matrix

H_{ρ}^* = the design model range measurement matrix

R_{ρ}^* = the design model range measurement noise covariance matrix

$H_{\dot{\rho}}^*$ = the design model range-rate measurement matrix

$R_{\dot{\rho}}^*$ = the design model range-rate measurement noise covariance matrix

B.2 THE 18-STATE INI KALMAN FILTER DESIGN MODEL

The elements of the 18-state filter state vector together with their assumed initial values were defined in Section 2.1. The remaining matrices required to complete the specification of this filter design model are presented in this subsection.

The 18-state dynamics matrix is based on the state vector as defined in Table 2.3-1. The resulting matrix is

$$F^* = \begin{array}{c} \begin{array}{ccc} 1-9 & 10 & 11-18 \end{array} \\ \left[\begin{array}{c|c|c} F_{11}^* & F_{12}^* & 0 \\ \hline 0 & 0 & 0 \\ \hline 0 & 0 & F_{33}^* \end{array} \right] \end{array} \quad (B.2-1)$$

where

$$F_{11}^* = F_{11} \quad (B.2-2)$$

$$F_{12} = \begin{bmatrix} 0 \\ 0 \\ D_2 \\ 0 \\ 0 \\ 0 \\ D_1 \\ 0 \\ 0 \\ 0 \end{bmatrix} \quad (B.2-3)$$

$$F_{33}^* = F_{55} \quad (\text{B.2-4})$$

The corresponding input noise covariance matrix for the 18-state filter is given by

$$Q^* = \begin{bmatrix} Q_{11}^* & 0 & 0 \\ 0 & 0 & 0 \\ 0 & 0 & Q_{33}^* \end{bmatrix} \quad (\text{B.2-5})$$

$$Q_{11}^* = \begin{bmatrix} 0 & 0 & 0 & 0 & 0 & 0 & 0 & 0 & 0 \\ 0 & 0 & 0 & 0 & 0 & 0 & 0 & 0 & 0 \\ 0 & 0 & q_3^* & 0 & 0 & q_{36}^* & 0 & 0 & 0 \\ 0 & 0 & 0 & q_4^* & 0 & 0 & 0 & 0 & 0 \\ 0 & 0 & 0 & 0 & q_5^* & 0 & 0 & 0 & 0 \\ 0 & 0 & q_{63}^* & 0 & 0 & q_6^* & 0 & 0 & 0 \\ 0 & 0 & 0 & 0 & 0 & 0 & q_7^* & 0 & 0 \\ 0 & 0 & 0 & 0 & 0 & 0 & 0 & q_8^* & 0 \\ 0 & 0 & 0 & 0 & 0 & 0 & 0 & 0 & q_9^* \end{bmatrix} \quad (\text{B.2-6})$$

and

$$Q_{33}^* = Q_{55} \quad (\text{B.2-7})$$

The elements of matrix Q_{11}^* are given below in Table B.2-1.

TABLE B.2-i
DIAGONAL ELEMENTS OF THE Q* MATRIX
FOR THE 15-STATE FILTER

Element	Value	Units
q^*_{36}	44.0	ft ² /sec
q^*_4, q^*_5	2.0×10^{-5}	ft ² /sec
q^*_6	1.3×10^{-2}	ft ² /s
q^*_7, q^*_8	4.0×10^{-6}	min ² /sec
q^*_9	2×10^{-5}	min ² /sec
q^*_{36}	0.75	ft ²

The measurement and measurement noise matrices for this filter are given as

$$H^*_{\rho_i} = \begin{bmatrix} 1 & 3 & 11 & 9 + 2i \\ \gamma_{Ni} & \gamma_{Ei} & \gamma_{Zi} & 0 \dots 1 \ 0 \dots \dots -k & 0 \dots \end{bmatrix} \quad (B.2-8)$$

where $k = 0$ for $i = 1$ and $k = 1$ for $i = 2, 3, 4$.

$$R^*_{\rho_i} = \left(\sigma^*_{\rho_i} \right)^2 \quad (B.2-9)$$

$$H^*_{\rho_i} = \begin{bmatrix} 1 & 6 & 7 & 12 & 10 + 2i \\ e_{Ni} & e_{Ei} & e_{Zi} & \gamma_{Ni} & \gamma_{Ei} & \gamma_{Zi} & 0 \dots 1 \ 0 \dots \dots -k & 0 \dots \end{bmatrix} \quad (B.2-10)$$

$$R_{\dot{\rho}_i}^* = \left(\sigma_{\dot{\rho}_i}^* \right)^2 \quad (\text{B.2-11})$$

Values for the white measurement noises are given in Table B.2-2.

TABLE B.2-2
DESIGN VALUES FOR 18-STATE FILTER
WHITE MEASUREMENT NOISES

Error	RMS Value
Range	8 ft
Range-Rate	1 ft/sec

REFERENCES

1. D'Appolito, J.A. and Roy, K.J., "Simulated Satellite/Inertial System Flight Test Support Studies", The Analytic Sciences Corporation, TR-213-2, 31 October 1971. (Confidential)
2. D'Appolito, J.A., "The Evaluation of Kalman Filter Designs for Multisensor Integrated Navigation Systems," The Analytic Sciences Corporation, AFAL-TR-70-271, January 1970.
3. "Platform Model for the A-7D/E Inertial Measurement Set" Document No. 6K032D025C, Kearfott Systems Division, General Precision Systems, Inc., Wayne, N.J., 29 March 1968.
4. Fine, T.I., "Integrated Inertial/Navsat Study Analysis and Planning for Test Final Report, Vol. 1. System Analysis," TRW Systems Group, Redondo Beach, Calif., AFAL-TR-71-319, Vol. 1. December 1971. (Confidential)
5. D'Appolito, J.A. and Roy, K.J., "Satellite/Inertial Navigation System Kalman Filter Design Study," The Analytic Sciences Corporation, AFAL-TR-71-178, June 1971. (Confidential)
6. "Development Specification, Operational Computer Program," Document No. Y202A010, Kearfott Division, Singer-General Precision, Inc., Little Falls, N.J., March 9, 1972.
7. "Integrated Navsat Inertial System Development Program General Test Plan (DRAFT)," TRW System Group, Redondo Beach, California, August 1972.
8. Newton, G. C., Jr., Gould, L.A., Kaiser, J.F., Analytical Design of Linear Feedback Controls, John Wiley & Sons, Inc., New York, 1957.

UNCLASSIFIED

Security Classification

DOCUMENT CONTROL DATA - R & D

(Security classification of title, body of abstract and indexing annotation must be entered when the overall report is classified)

1. ORIGINATING ACTIVITY (Corporate author) THE ANALYTIC SCIENCES CORPORATION 6 Jacob Way Reading, Massachusetts 01867		2a. REPORT SECURITY CLASSIFICATION UNCLASSIFIED	
		2b. GROUP N/A	
3. REPORT TITLE Integrated Navigation Satellite/Inertial Flight Test Analysis			
4. DESCRIPTIVE NOTES (Type of report and inclusive dates) Technical Report (March 1972 through January 1973)			
5. AUTHOR(S) (First name, middle initial, last name) Joseph A. D'Appolito Kenneth J. Roy			
6. REPORT DATE 5 April 1973		7a. TOTAL NO. OF PAGES 70	7b. NO. OF REFS 8
8a. CONTRACT OR GRANT NO. F33615-72-C-1918		9a. ORIGINATOR'S REPORT NUMBER(S) TR-332-1	
b. PROJECT NO.			
c.		9b. OTHER REPORT NO(S) (Any other numbers that may be assigned this report) AFAL-TR-73-242	
d.			
10. DISTRIBUTION STATEMENT Distribution is limited to U.S. Government Agencies only. Reason: Test and Evaluation, Date Statement Applied: June 1973. Other requests for this document must be referred to: AFAL (NVA/666A), WPAFB, Ohio 45433			
11. SUPPLEMENTARY NOTES		12. SPONSORING MILITARY ACTIVITY Air Force Avionics Laboratory, Air Force Systems Command, Wright-Patterson AFB, Ohio 45433	
13. ABSTRACT <p>A simulation of an integrated airborne 621B Satellite/Inertial navigation system is planned in which a ground-based beacon configuration will be used in place of the satellites. The TRW Systems Group has designed and built an Integrated Navigation Satellite/Inertial (INI) system and will participate in a test of this equipment for the Air Force Avionics Laboratory at the White Sands Missile Range test center.</p> <p>This study represents a continuation of an earlier INI flight support study conducted by TASC. In this study the INI reference system model is first revised to include the most current data on inertial system and beacon errors. Then an 18-state INI Kalman filter for integrating beacon receiver and inertial data is described. The filter is evaluated in a performance study which includes a comparison against an optimally integrated INI system using a complete 33-state reference error model. Special attention is focused on the conventional barometer damped vertical channel mechanization proposed by TRW and the problem of filter initialization. A component error budget is generated for the 18-state Kalman filter to identify major sources of system error and filter sensitivity to those errors. A brief review of the TRW flight test program is then presented. An 18-state INI Kalman filter is recommended for initial use in the flight tests and certain additions to the real time flight test data display and diagnostics are suggested.</p>			

DD FORM 1473

1 NOV 65

UNCLASSIFIED

Security Classification

UNCLASSIFIED

Security Classification

14. KEY WORDS	LINK A		LINK B		LINK C	
	ROLE	WT	ROLE	WT	ROLE	WT
Satellite/Inertial navigation Beacon/Inertial navigation Multisensor navigation Applied Kalman filtering Radio satellite navigation DNSS DNSDP INI INHI						

UNCLASSIFIED

Security Classification